Validation of Shell Ionization Cross Sections for Monte Carlo Electron Transport

Tullio Basaglia, Matteo Bonanomi, Federico Cattorini, Min Cheol Han, Gabriela Hoff, Chan Hyeong Kim, Sung Hun Kim, Matteo Marcoli, Maria Grazia Pia, and Paolo Saracco

***Abstract*— Theoretical and semi-empirical methods to calculate electron impact ionization cross sections for atomic shells are subject to validation tests with respect to a wide collection of experimental measurements to identify the state of the art for Monte Carlo particle transport. The validation process applies rigorous statistical analysis methods. Cross sections based on the EEDL Evaluated Electron Data Library, widely used by Monte Carlo codes, and on calculations by Bote and Salvat, used in the Penelope code, are generally equivalent in compatibility with experiment. Results are also reported for various formulations of the Binary-Encounter-Bethe and Deutsch-Märk models.**

***Index Terms*— Cross sections, Geant4, ionization, Monte Carlo simulation, software validation.**

I. Introduction

THE study reported in this paper complements a previous investigation [1] of ionization cross sections for electron transport with respect to experimental data: the previous publication examined total cross sections, with special emphasis on the low energy range up to a few keV, while the present study concerns the ionization of atomic inner shells by electron impact. Both studies aim to identify the state of the art for the calculation of electron ionization cross sections in Monte Carlo transport codes.

Modeling electron interactions with matter is a fundamental task of any particle transport code. The ability to calculate cross sections for the ionization of individual shells, along with the capability to simulate the subsequent atomic relaxation [2], [3], is required in a variety of experimental environments: in materials analysis performed by electron-probe microanalysis, in surface analysis performed through Auger electron spectroscopy and more generally in experimental scenarios where the simulation of characteristic X-ray or Auger electron emission is important.

Theoretical and semi-empirical models have been developed over several decades to calculate electron impact ionization cross sections for atomic shells; nevertheless, despite the experimental relevance of these cross sections, limited documentation is available in the literature about quantitative validation of their calculations. Comparisons with experimental data, such as those concerning the Deutsch-Märk model [4], often rest on the visual appraisal of plots only. A recent publication [5] illustrates comparisons between some theoretical calculations and experimental data published up to May 2013; however, it is limited to the domain of descriptive statistics, lacking statistical inference. Objective quantification is also missing in the assessment of the relative merits of the various calculation methods: their relative ability to reproduce experimental measurements has not been estimated with statistical methods yet.

This paper evaluates quantitatively and objectively the capabilities of several calculation methods of electron impact ionization cross sections that are relevant for general purpose Monte Carlo transport codes. The evaluation concerns K shell, L and M subshell ionization cross sections, for which experimental measurements are reported in the literature. Statistical inference is applied both to validate cross section calculations with respect to experimental measurements and to detect significant differences in the ability of the various calculations to reproduce experiment. The outcome of this process identifies the state of the art in modeling electron impact ionization cross sections for K, L and M shells in Monte Carlo particle transport codes.

II. Electron Impact Ionization Cross Sections

The validation study reported in this paper addresses the calculation of electron impact ionization cross sections in a pragmatic way, i.e. considering calculation methods that are sustainable within the computational constraints of particle transport codes, either by implementing simple analytical formulations or by interpolating available tabulations of theoretical cross section calculations. Since the focus is on general-purpose Monte Carlo codes, only methods able to calculate electron impact ionization for any shell, and covering an extended electron energy range, are considered in the validation tests.

Manuscript received April 24, 2018; revised June 22, 2018; accepted June 27, 2018. Date of publication June 29, 2018; date of current version August 15, 2018.

T. Basaglia is with CERN, CH-1211 Geneva, Switzerland (e-mail: tullio.basaglia@cern.ch).

M. Bonanomi, F. Cattorini, and M. Marcoli are with the University of Milano-Bicocca, 20126 Milan, Italy (e-mail: m.bonanomi@campus.unimib.it; f.cattorini@campus.unimib.it; m.marcoli@campus.unimib.it).

M. C. Han, M. G. Pia, and P. Saracco are with the INFN Sezione di Genova, 16146 Genova, Italy (e-mail: mincheol.han@ge.infn.it; mariagrazia.pia@ge.infn.it; paolo.saracco@ge.infn.it).

G. Hoff is with the University of Cagliari, Monserrato, Italy, and also with the INFN Sezione di Cagliari, 09042 Monserrato, Italy (e-mail: ghoff.gesic@gmail.com).

C. H. Kim and S. H. Kim are with the Department of Nuclear Engineering, Hanyang University, Seoul 133-791, South Korea (e-mail: chkim@hanyang.ac.kr; ksh4249@hanyang.ac.kr).

Color versions of one or more of the figures in this paper are available online at http://ieeexplore.ieee.org.

Digital Object Identifier 10.1109/TNS.2018.2851921

TABLE I
CROSS SECTION CALCULATION METHODS EVALUATED IN THE VALIDATION TEST

Model	Identifier	Type	Reference
EEDL	EEDL	Tabulation	[6]
EEDL, EPICS2017	EPICS2017	Tabulation	[23]
EEDL, Geant4 4.1-10.4	EEDLG4	Tabulation	-
Bote-Salvat, Penelope2014	Bote	Tabulation	[7]
Bote-Salvat, NIST-164	NIST164	Tabulation	[31]
Binary-Encounter-Bethe	BEB	Analytical	[10]
Binary-Encounter-Bethe, average	BEBav	Analytical	[33], [34]
Binary-Encounter-Bethe, relativistic	BEBR	Analytical	[33]
Deutsch-Märk	DM	Analytical	[35]–[37]
Deutsch-Märk, 2000 version	DM2000	Analytical	[4], [38]
Deutsch-Märk, modified relativistic	DMMR	Analytical	[39]

The cross sections evaluated in this paper include two sets of tabulations derived from theoretical calculations, EEDL (Evaluated Electron Data Library) [6] and the data tables based on [7], and two analytical models that especially address the low energy range (below a few keV), which were included in the previous validation test of total electron ionization cross sections [1]: the Binary Encounter Bethe (BEB) model [10] and the Deutsch-Märk (DM) model [11]. Various versions of the data libraries and variants of the analytical models are examined. The cross sections subject to test are summarized in Table I.

Several other empirical or semi-empirical formulae have been documented in the literature for the calculation of electron impact ionization cross sections, such as the classical model developed by Gryzinski [12] and the formulae developed by Casnati [13] and Kolbenstvedt [14] for K shell ionization. Due to the limitations of their applicability, either concerning the incident electron energy or the ionized shell, these analytical formulae are not well suited to modern, general-purpose Monte Carlo simulation codes, which require physics models able to address a large variety of experimental scenarios. Models with limited scope are not considered in this validation test.

A. EEDL Evaluated Electron Data Library

The EEDL data library, originally distributed by Lawrence Livermore National Laboratory (LLNL), is widely used by Monte Carlo particle transport codes. The cross sections tabulated in EEDL [6] are based on Seltzer's calculation method [15], which distinguishes close and distant collisions. For close collisions, EEDL uses Seltzer's modification of the Møller [17] binary collision cross section, which takes into consideration the binding of the atomic electron in a given subshell; for distant collisions it uses Seltzer's modification of the Weizsäcker-Williams [16], [18] method. The atomic parameters required in these calculations were taken from EADL (Evaluated Atomic Data Library) [19], while the subshell photoelectric cross sections required for the distant-collision component were derived from the 1989 version of EPDL (Evaluated Photon Data Library) [20], [21]. EEDL tabulations cover the energy range from 5 eV to 100 GeV.

The latest release of EEDL by LLNL, identified in this paper as EEDL, dates back to 1991. Since 2014 the IAEA (International Atomic Energy Agency) has distributed a collection of data libraries named EPICS, which includes EEDL along with EADL and EPDL. The cross sections for shell ionization by electron impact included in EPICS2014 [22] are identical to those originally released in EEDL in 1991; therefore, they are not considered in the validation process documented in this paper.

Modified cross sections for shell ionization by electron impact were released in January 2018 in the EEDL library [23] of EPICS2017; they are identified in the following sections as EPICS2017. The values of the cross sections tabulated in EPICS2017 are the same as in the original EEDL, but they are associated with different electron energies to account for modified atomic binding energies in the EADL [24] library of EPICS2017. The documentation of EPICS2017 [23] states that the EEDL cross section tabulations have been extended to include about three times as many data to be suitable for linear interpolation; nevertheless, the same number of cross section data for shell ionization by electron impact is tabulated in EPICS2017, EPICS2014 and EEDL1991. Cross sections calculated from linear interpolation of EPICS2017 tabulations are identified in this validation test as EPICS2017lin; otherwise, cross sections identified as EPICS2017 derive from logarithmic interpolation.

EEDL is also distributed within other nuclear data libraries, such as ENDF/B-VII.1 [25] and JENDL-4.0 [26]. The same ionization cross sections as in EPICS2017 are included in the electro-atomic data library of ENDF/B-VIII.0 [27].

EEDL ionization cross sections are distributed in the Geant4 [28]–[30] toolkit in a modified format; until Geant4 version 4.0 the cross sections for shell ionization by electron impact are the same as in the original EEDL 1991 [6], while different tabulations are associated with Geant4 versions from 4.1 to 10.4 (the most recent one at the time of writing this paper). These tabulations, whose origin does not appear to be documented, are identified in the following as EEDLG4.

B. Bote and Salvat Calculations

Theoretical calculations by Bote and Salvat [7] combine the relativistic plane wave Born approximation (PWBA) with a semi-relativistic version of the distorted wave Born approximation (DWBA).

Tabulations based on these calculations can be produced through a Java code available as "NIST Standard Reference Database 164" [31] from NIST (National Institute of Standard and Technology). Data tables based on [7], which cover the energy range from approximately 10 eV to 1 GeV, are also distributed with the Penelope 2014 [32] Monte Carlo code. Cross section calculations based on Penelope 2014 and NIST Standard Reference Database 164 are identified in this paper as Bote and NIST164, respectively.

An analytical parameterization of Bote and Salvat calculations is documented in [8], followed two years later by an erratum [9] describing empirical corrections to account for the effects of theoretically derived ionization energies, which

TABLE II
SUMMARY OF EXPERIMENTAL K SHELL CROSS SECTIONS

Z	Element	E_{min}	E_{max}	N_{data}	References
1	H	13.5 eV	4 keV	292	[40]–[44]
2	He	20 eV	20 keV	404	[45]–[54]
6	C	0.29 keV	80 keV	62	[55]–[60]
7	N	0.45 keV	25 keV	57	[56], [58], [60], [61]
8	O	0.63 keV	25 keV	77	[56], [58]–[63]
10	Ne	0.95 keV	14.6 keV	39	[60]–[62]
11	Na	1.2 keV	230 MeV	13	[56], [64]
12	Mg	10 MeV	230 MeV	5	[64]–[66]
13	Al	1.63 keV	230 MeV	90	[59], [63]–[72]
14	Si	2.5 keV	150 MeV	34	[59], [62], [65], [69], [73], [74]
16	S	7 keV	30 keV	24	[75]
17	Cl	6 keV	270 MeV	19	[64], [69], [76]
18	Ar	3.2 keV	60 MeV	81	[60], [62], [65], [77]–[81]
19	K	3.75 keV	45 keV	30	[82], [83]
20	Ca	4.5 keV	270 MeV	55	[65], [69], [70], [75], [82]
21	Sc	4.8 keV	45 keV	36	[84]–[86]
22	Ti	5.5 keV	300 MeV	77	[59], [72], [85], [87]–[91]
23	V	5.9 keV	2 MeV	47	[84]–[86], [90], [92]
24	Cr	5.5 keV	60 MeV	107	[65], [85], [87], [88], [90], [92]–[95]
25	Mn	6.75 keV	350 MeV	100	[65], [85], [90]–[92], [96]–[101]
26	Fe	7.35 keV	2 MeV	90	[85], [92], [96], [98], [99], [102], [103]
27	Co	8.1 keV	2 MeV	29	[70], [85], [92], [104]
28	Ni	6.3 keV	2 GeV	147	[65], [85], [88]–[90], [92]–[97], [105]–[111]
29	Cu	6.7 keV	2 GeV	138	[63], [65], [69], [72], [85], [88], [91]–[94], [96], [97], [100], [104], [107], [113]–[118]
30	Zn	9.7 keV	150 MeV	51	[69], [75], [85], [90], [92], [101]
31	Ga	10.5 keV	39 keV	51	[118]–[120]
32	Ge	10.6 keV	60 MeV	77	[65], [85], [117], [120]–[122]
33	As	12 keV	39 keV	28	[119]
34	Se	13 keV	380 MeV	36	[69], [85], [91], [92], [97], [113], [123], [124]
35	Br	2 MeV	2 MeV	1	[92]
36	Kr	20 MeV	60 MeV	10	[65], [79]
37	Rb	16 keV	2 MeV	12	[82], [92]
38	Sr	17 keV	900 MeV	15	[82], [92], [116]
39	Y	18 keV	380 MeV	20	[65], [69], [85], [91], [110], [124]
40	Zr	20 keV	1.44 MeV	14	[72], [120], [125]
41	Nb	20 keV	34 keV	15	[85], [126]
42	Mo	19.2 keV	900 MeV	37	[69], [85], [103], [116], [127]
46	Pd	300 keV	250 MeV	8	[69], [128], [129]
47	Ag	26 keV	2 GeV	147	[65], [72], [91], [92], [97], [106]–[108], [110], [114], [115], [117], [123], [129]–[138]
48	Cd	2 MeV	2 MeV	1	[92]
49	In	300 keV	900 MeV	11	[69], [92], [116], [129]
50	Sn	47.1 keV	380 MeV	53	[63], [65], [69], [91], [92], [97], [108], [125], [129], [131], [133]
51	Sb	60 keV	2 MeV	9	[72], [92], [123]
52	Te	2 MeV	380 MeV	3	[91], [92]
54	Xe	20 MeV	60 MeV	10	[65], [79]
56	Ba	100 keV	270 MeV	6	[69], [72], [92]
57	La	100 keV	2 MeV	2	[72], [92]
58	Ce	2 MeV	2 MeV	1	[92]
59	Pr	100 keV	2 MeV	2	[72], [92]
60	Nd	2 MeV	2 MeV	1	[92]
62	Sm	2 MeV	90 MeV	2	[69], [92]
63	Eu	2 MeV	2 MeV	1	[92]
64	Gd	2 MeV	2 MeV	1	[92]
67	Ho	20 MeV	90 MeV	3	[65], [69]
68	Er	2 MeV	2 MeV	1	[92]
69	Tm	300 MeV	900 MeV	4	[116]
70	Yb	490 keV	2 MeV	3	[92], [110]
73	Ta	490 keV	500 MeV	4	[110], [116]
74	W	209 keV	1.44 MeV	12	[125], [131]
78	Pt	2 MeV	2 MeV	1	[92]
79	Au	82.9 keV	900 MeV	73	[63], [65], [69], [92], [106], [108], [110], [114], [116], [128], [131], [133], [139]
82	Pb	240 keV	90 MeV	16	[65], [69], [92], [110], [125], [131]
83	Bi	92 keV	500 MeV	12	[65], [69], [92], [116], [139]
92	U	90 MeV	90 MeV	1	[69]

differ from experimental values. Although a parameterization may be useful in cases where an analytical approximation is preferred to a large numerical database, the involved correction documented in [9], which is left to the user's responsibility, discourages its use in experimental practice; therefore, it is not considered in the validation process.

TABLE III
SUMMARY OF EXPERIMENTAL L_1 SUBSHELL CROSS SECTIONS

Z	Element	E_{min}	E_{max}	N_{data}	References
29	Cu	50 keV	100 keV	2	[140]
38	Sr	50 keV	200 keV	4	[140]
47	Ag	6 keV	150 keV	21	[140], [141]
50	Sn	200 keV	200 keV	1	[140]
54	Xe	6.28 keV	14.27 keV	6	[142]
56	Ba	1.04 MeV	1.76 MeV	3	[143]
57	La	1.04 MeV	1.76 MeV	3	[143]
58	Ce	1.04 MeV	1.76 MeV	3	[143]
59	Pr	1.04 MeV	1.76 MeV	3	[143]
60	Nd	1.04 MeV	1.76 MeV	3	[143]
62	Sm	50 keV	1.76 MeV	6	[140], [143]
63	Eu	1.04 MeV	1.76 MeV	3	[143]
64	Gd	1.04 MeV	1.76 MeV	3	[143]
68	Er	1.04 MeV	1.76 MeV	3	[143]
70	Yb	1.04 MeV	1.76 MeV	3	[143]
73	Ta	50 keV	150 keV	3	[140]
74	W	15 keV	40 keV	10	[144]
75	Re	1.04 MeV	1.76 MeV	3	[143]
78	Pt	1.04 MeV	1.76 MeV	3	[143]
79	Au	16 keV	600 keV	26	[145]–[147]
82	Pb	18 keV	1.76 MeV	20	[143], [146], [148]
83	Bi	60 keV	1.76 MeV	10	[143], [146]
90	Th	27.5 keV	45 keV	8	[148]

TABLE IV
SUMMARY OF EXPERIMENTAL L_2 SUBSHELL CROSS SECTIONS

Z	Element	E_{min}	E_{max}	N_{data}	References
29	Cu	50 keV	100 keV	2	[140]
38	Sr	50 keV	200 keV	4	[140]
47	Ag	6 keV	150 keV	21	[140], [141]
50	Sn	200 keV	200 keV	1	[140]
54	Xe	5.74 keV	14.3 keV	14	[142]
56	Ba	1.04 MeV	1.76 MeV	3	[143]
57	La	1.04 MeV	1.76 MeV	3	[143]
58	Ce	1.04 MeV	1.76 MeV	3	[143]
59	Pr	1.04 MeV	1.76 MeV	3	[143]
60	Nd	1.04 MeV	1.76 MeV	3	[143]
62	Sm	50 keV	1.76 MeV	6	[140], [143]
63	Eu	1.04 MeV	1.76 MeV	3	[143]
64	Gd	1.04 MeV	1.76 MeV	3	[143]
68	Er	1.04 MeV	1.76 MeV	3	[143]
70	Yb	1.04 MeV	1.76 MeV	3	[143]
73	Ta	50 keV	150 keV	3	[140]
74	W	13 keV	40 keV	11	[144]
75	Re	1.04 MeV	1.76 MeV	3	[143]
78	Pt	1.04 MeV	1.76 MeV	3	[143]
79	Au	14.7 keV	600 keV	68	[145]–[147], [149]–[154]
82	Pb	18 keV	1.76 MeV	20	[143], [146], [148]
83	Bi	60 keV	1.76 MeV	10	[143], [146]
90	Th	25 keV	45 keV	9	[148]

C. Binary-Encounter-Bethe Model

The Binary-Encounter-Bethe (BEB) model is a simplified version of the Binary-Encounter-Dipole model [10] of electron impact ionization cross sections, which combines a modified form of the Mott cross section with the Bethe theory. It is especially intended for low energy electrons.

Modified versions of this model, such as the relativistic BEB model (BEBR) [33] and the average BEB formula (BEBav) [33], [34], have been proposed to describe single ionization of tightly bound inner shells.

D. Deutsch-Märk Model

The Deutsch-Märk (DM) model has a phenomenological character: it originates from a classical binary encounter approximation and incorporates parameters determined from a fit to experimental data. It was subject to several evolutions; the latest formulation and associated parameters available at the time of writing this paper are documented in [35]–[37].

TABLE V
SUMMARY OF EXPERIMENTAL L_3 SUBSHELL CROSS SECTIONS

Z	Element	E_{min}	E_{max}	N_{data}	References
29	Cu	50 keV	100 keV	2	[140]
38	Sr	50 keV	200 keV	4	[140]
47	Ag	6 keV	150 keV	21	[140], [141]
50	Sn	200 keV	200 keV	1	[140]
54	Xe	4.79 keV	14 keV	35	[78], [142]
56	Ba	1.04 MeV	1.76 MeV	3	[143]
57	La	1.04 MeV	1.76 MeV	3	[143]
58	Ce	1.04 MeV	1.76 MeV	3	[143]
59	Pr	1.04 MeV	1.76 MeV	3	[143]
60	Nd	1.04 MeV	1.76 MeV	3	[143]
62	Sm	50 keV	1.76 MeV	6	[140], [143]
63	Eu	1.04 MeV	1.76 MeV	3	[143]
64	Gd	1.04 MeV	1.76 MeV	3	[143]
68	Er	1.04 MeV	1.76 MeV	3	[143]
70	Yb	1.04 MeV	1.76 MeV	3	[143]
73	Ta	50 keV	150 keV	3	[140]
74	W	11 keV	40 keV	11	[144]
75	Re	1.04 MeV	1.76 MeV	3	[143]
78	Pt	1.04 MeV	1.76 MeV	3	[143]
79	Au	12.3 keV	600 keV	122	[114], [117], [135], [136], [145]–[147], [149]–[154]
82	Pb	16 keV	1.76 MeV	21	[143], [146], [148]
83	Bi	60 keV	1.76 MeV	10	[143], [146]
90	Th	20 keV	45 keV	11	[148]

TABLE VI
SUMMARY OF EXPERIMENTAL M SHELL CROSS SECTIONS

Subshell	Z	Element	E_{min}	E_{max}	N_{data}	References
M_1	18	Ar	0.03 keV	1 keV	31	[155]
	92	U	6 keV	38 keV	33	[156]
M_2	36	Kr	0.25 keV	3 keV	19	[157]
	92	U	5 keV	38 keV	35	[156]
M_3	36	Kr	0.25 keV	3 keV	20	[157]
	92	U	4 keV	38 keV	34	[156]
M_4	92	U	4 keV	38 keV	34	[156]
M_5	92	U	4 keV	38 keV	34	[156]

The validation test also includes cross sections calculated according to an earlier formulation of the Deutsch-Märk model reported in [4], with associated parameters documented in [38]. These cross sections are identified in the following as DM2000.

A modified version of the DM model [39] was specifically formulated for the K shell; it is identified as DMMR in the following analysis.

III. REFERENCE DATA SOURCES

A. Ionization Cross Section Measurements

Experimental data were gathered from the literature; the data collection [40]–[158] includes measurements published by the end of 2017. Tables II–VI summarize the main features of the collected experimental data samples for the K shell, the L_1, L_2, L_3 and M subshells, respectively; they list the atomic number (Z) and the symbol of the measured element,

the energy range ($E_{\min}$, $E_{\max}$) of the data and the number (N_{data}) of experimental measurements.

Experimental ionization cross sections are mainly derived by measuring the cross section for the production of X-rays or Auger electrons, which are emitted when bound electrons fill the vacancy created by electron impact. However, these measurements may not truly represent electron impact ionization, unless experimental measurements have explicitly excluded the contribution from vacancies created by excitation: for instance, K-shell vacancies can be created not only by direct ionization, but also by excitations of K electrons to unoccupied bound states. Since the cross section models considered in this validation test account only for direct ionization, there may be an intrinsic discrepancy between theory and experiment due to neglecting excitation.

Additional systematic effects may derive from the conversion of measured cross sections for the production of X-rays or Auger electrons into ionization cross sections: this procedure involves atomic parameters, which are affected by uncertainties and could introduce systematic effects in the calculation. A discussion of this subject is summarized in Section III-B.

Experimental data were evaluated for correctness and consistency prior to their use in the validation process. They were visually inspected to identify factual errors (e.g. typographic errors in the published values), manifest inconsistencies and systematic effects, such as experimental cross sections that are systematically larger or smaller than those measured by other experiments. The Wald-Wolfowitz test [159] was applied when visual appraisal was not sufficient to ascertain the systematic nature of apparent inconsistencies.

Experimental uncertainties are not documented in some publications, or are partially documented, e.g. limited to statistical errors; uncertainties equivalent to those reported by experiments operating in similar conditions were associated with these data. To mitigate the risk of incorrect estimates of experimental uncertainties, the validation process involved different type of tests for statistical inference: the χ^2 test [160], which takes into account experimental uncertainties explicitly in the formulation of the test statistic, and goodness-of-fit tests based on the empirical distribution function, whose formulation does not involve experimental errors explicitly. The analysis strategy is documented in detail in Section V.

Experimental cross sections published only in graphs were digitized by means of the Engauge [161] and PlotDigitizer [162] software. The digitization process represents an additional source of errors, which can be especially significant at energies where rapid variations of the cross section are observed. Data close to threshold were not digitized due to the difficulty of reliably reproducing their values and realistic uncertainties. Apart from these critical cases, the error associated with the digitization process was estimated by digitizing data published both in graphical and numerical form.

Measurements near threshold were also discarded from the analysis when their uncertainties appeared underestimated (e.g. comparable to those of less sensitive measurements), presumably due to the absence of sensitivity analysis related to the primary electron energy.

TABLE VII
FLUORESCENCE YIELDS COMPILATIONS

Reference	Year	Atomic Number	Identifier
Bambynek [163]	1972	13-80, 82, 92	Bambynek1972
Bambynek [173]	1984	3-99	Bambynek1984
Daoudi [167]	2015	3-99	Daoudi
EADL [19]	1991	6-100	EADL
Elam [168]	2002	3-98	Elam
Hubbell [172]	1989	2-110	Hubbell1989
Hubbell [165],[166]	1994	3-110	Hubbell1994
Kahoul [169]	2011	6-99	Kahoul F_1, F_3, F_4, F_5
Kahoul [170]	2012	11-99	Kahoul2012
Krause [164]	1979	5-110	Krause
XOP 2.4 [171]	2013	4-91	XOP

B. Fluorescence Yields

Fluorescence yields represent the probability of a core hole in an atomic shell being filled by a radiative process, in competition with non-radiative processes (Auger and Coster-Kronig transitions). The K shell ionization cross section σ_I is related to the K shell X-ray production cross section σ_X by the K shell fluorescence yield ω_K as

$$\sigma_X = \omega_K \sigma_I. \tag{1}$$

More complex equations, which involve additional atomic parameters, relate the X-ray production and ionization cross sections of outer shells.

Several compilations of fluorescence yields are available in the literature; some of them simply assemble existing experimental data on the basis of some quality evaluation, while others provide semi-empirical calculations as a function of the atomic number, usually derived from fits to experimental data; other compilations are based on theoretical calculations. The most common sources of fluorescence yields in experimental practice are the compilations by Bambynek (1972 version) [163], Krause [164] and Hubbell [165], [166]. Some modern compilations (e.g. [167]–[170]), which adopted a similar semi-empirical approach, are based on more extensive experimental collections including recent measurements. Fluorescence yields are also distributed in EADL and in XOP (X-ray Oriented Programs) [171].

The sources of fluorescence yields considered in this study are summarized in Table VII. The values reported in [172] appear to be identical to those previously published in [173]; therefore the results based on this compilation are not discussed in Section VI. Several semi-empirical formulations to calculate fluorescence yields are documented in [169]; they appear in the following analysis as Kahoul F_1, F_3, F_4, F_5, where the subscript identifies the number of the corresponding equation in the publication.

IV. CROSS SECTION CALCULATION

All the cross section models included in the validation test have been implemented in a consistent software design, compatible with the Geant4 toolkit. The software adopts a policy-based class design [174], as this technique enables the development of a wide variety of calculation methods with

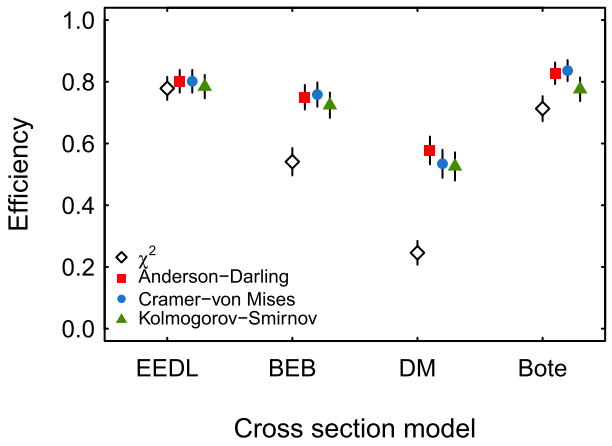

Fig. 1. Efficiency of K shell cross section models obtained with different goodness-of-fit tests in the energy range between 1 keV and 1 MeV: χ^2 (empty diamonds), Anderson-Darling (red squares), Cramer-von Mises (blue circles) and Kolmogorov-Smirnov (green triangles) tests.

minimal dependencies, thus facilitating the configuration of validation tests. The software design and the implementation of BEB, DM and EEDL cross section calculations are described in detail in [1].

Additional analytical calculations corresponding to variants of the BEB and DM models (BEBav, BEBR, DM2000, DMMR) have been implemented in dedicated policy classes. The correctness of the software implementation has been verified through comparison with published values. The concepts and actions pertaining to the verification and validation processes are documented in [175].

The same policy class is used to calculate cross sections based on the interpolation of tabulated values: Bote, EEDL, EEDLG4, EPICS2017 and NIST164. Logarithmic interpolation is applied, as recommended in [6], unless otherwise specified.

V. Data Analysis

The analysis is articulated over three stages, which apply pertinent methods of statistical inference.

The first stage consists of validation tests, which evaluate the compatibility between the cross sections calculated by the various models and experimental measurements by means of two-sample goodness-of-fit tests. Validation test cases are defined by grouping the measurements performed by each experiment in well identified configurations: with a fixed target element as a function of energy, or with fixed primary electron energy as a function of the atomic number of the target.

For convenience, the outcome of goodness-of-fit (GoF) tests is summarized over all test cases by a variable denoted as "efficiency," which is defined as the fraction of test cases in which a given test does not reject the null hypothesis (i.e. the hypothesis of equivalence of calculated and measured cross section distributions). The uncertainties on the efficiencies are calculated both with the conventional method involving the binomial distribution [176] and with a method based on Bayes' theorem [177], [178]. The latter delivers meaningful results in

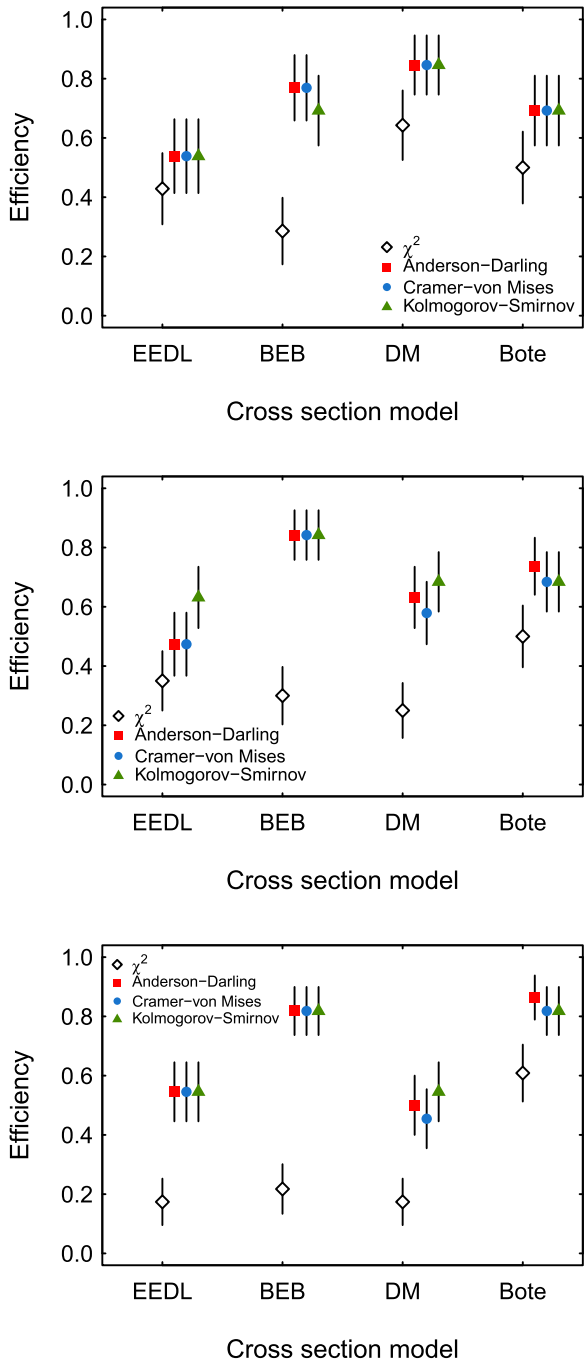

Fig. 2. Efficiency of cross section models obtained with different goodness-of-fit tests in the energy range between 1 keV and 1 MeV for L_1 (top), L_2 (middle) and L_3 (bottom) subshells: χ^2 (empty diamonds), Anderson-Darling (red squares), Cramer-von Mises (blue circles) and Kolmogorov-Smirnov (green triangles) tests.

extreme cases, i.e. for efficiencies very close to 0 or to 1, where the conventional method produces unreasonable values; otherwise both methods deliver identical results within the number of significant digits reported in this paper. The uncertainties reported in this paper are calculated according to [177], [178].

In the second stage, categorical data analysis determines whether significant differences in compatibility with

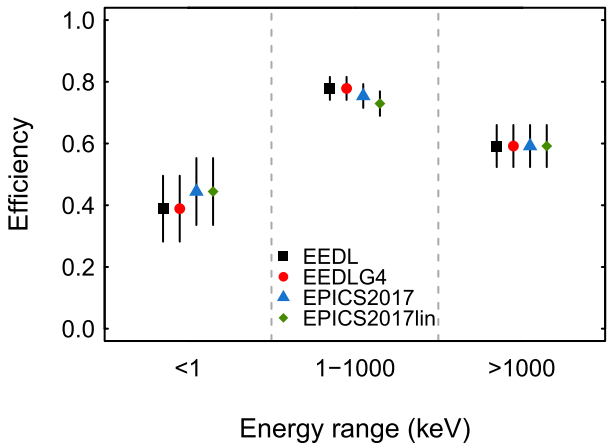

Fig. 3. Efficiency of K shell cross section calculations based on different versions and interpolations of the EEDL data library, resulting from the χ^2 goodness-of-fit test, in three energy ranges (below 1 keV, between 1 keV and 1 MeV, and above 1 MeV): EEDL 1991 version (black squares), EEDL used in Geant4 versions 4.1 to 10.4 (red circles), and as in EPICS 2017 with logarithmic (blue triangles) or linear (green diamonds) interpolation.

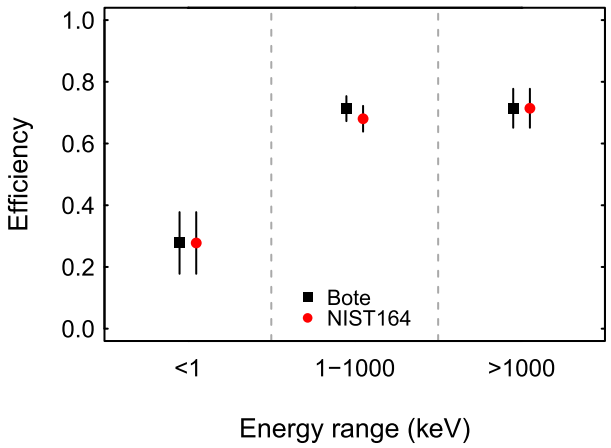

Fig. 5. Efficiency of K shell cross section calculations based on different tabulations of Bote and Salvat calculations, resulting from the χ^2 goodness-of-fit test, in three energy ranges (below 1 keV, between 1 keV and 1 MeV, and above 1 MeV): tabulations as in Penelope 2014 (black squares) and produced by NIST Standard Database 164 (red circles).

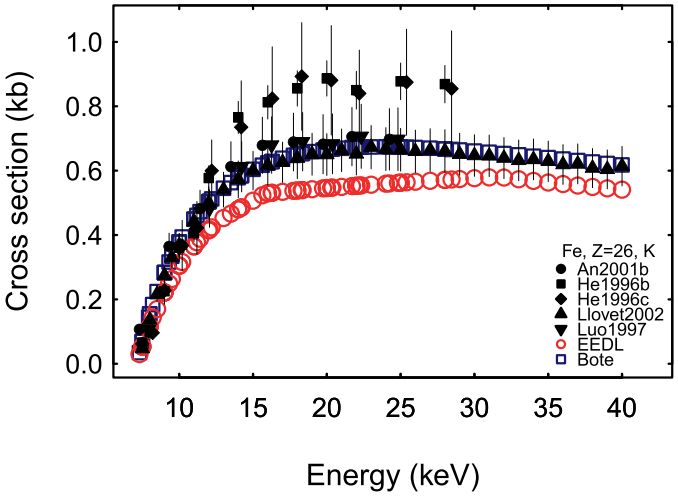

Fig. 4. Example of effects related to the characteristics of tabulated cross sections: both Bote (blue empty squares) and EEDL (red empty circles) tabulated cross sections are logarithmically interpolated with the same software implementation of the same algorithm, nevertheless the cross sections interpolated from EEDL appear as straight segments above approximately 15 keV as an effect of the coarse granularity of their tabulations as a function of energy. Experimental data are represented by black markers.

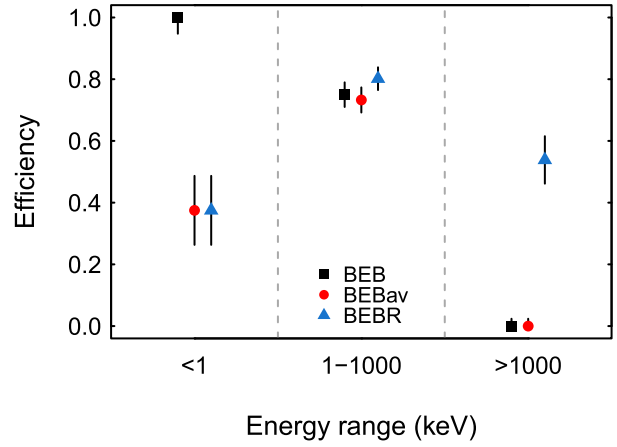

Fig. 6. Efficiency of K shell cross section calculations based on different formulations of the Binary-Encounter-Bethe model, resulting from the Anderson-Darling goodness-of-fit test, in three energy ranges (below 1 keV, between 1 keV and 1 MeV, and above 1 MeV): the original version of the model [10] (black squares), the average BEB formula [33], [34] (red circles) and the relativistic BEB model (BEBR) [33] (blue triangles).

experiment are present among the cross section models. Contingency tables, reporting the number of test cases where the null hypothesis is rejected or not rejected by goodness-of-fit tests, are built to compare the performance of the various cross section calculations with respect to that of the most recent theoretical approach of Bote. Due to the small number of experimental measurements concerning M subshells available in the literature, this analysis is meaningful only for K and L shell cross sections.

A variety of statistical tests is applied at each stage of the analysis to mitigate the risk of introducing systematic effects related to the mathematical formulation of the test statistic: the χ^2 [160], Anderson-Darling [179], [180] (identified in the following tables as AD), Cramer-von Mises [181], [182] and Kolmogorov-Smirnov [183], [184] goodness-of-fit tests are used to evaluate the compatibility of calculated cross sections with experimental measurements; Pearson's χ^2 test [185], Fisher exact test [186], Barnard test (using the Z-pooled statistic [187] and the CSM formulation [188]) and Boschloo test [189] are used to analyze contingency tables. The significance level of the tests is set at 0.01, unless otherwise specified.

The third stage of the analysis addresses the investigation of possible systematic effects in the validation process related to the derivation of ionization cross sections from measurements of X-ray production cross sections. It is performed only for K shell cross sections, for which a sufficiently large experimental data sample allows refined statistical investigations; moreover,

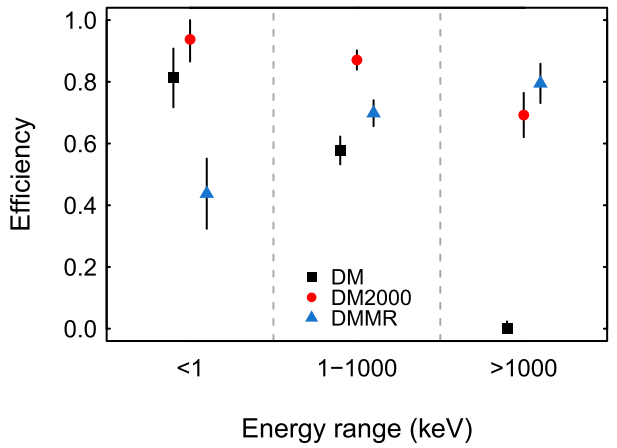

Fig. 7. Efficiency of K shell cross section calculations based on different formulations of the Deutsch-Märk model, resulting from the Anderson-Darling goodness-of-fit test, in three energy ranges (below 1 keV, between 1 keV and 1 MeV, and above 1 MeV): the most recent version of the model documented in [35]–[37] (black squares), an earlier version [4], [38] (red circles), and the relativistic version of [39] (blue triangles).

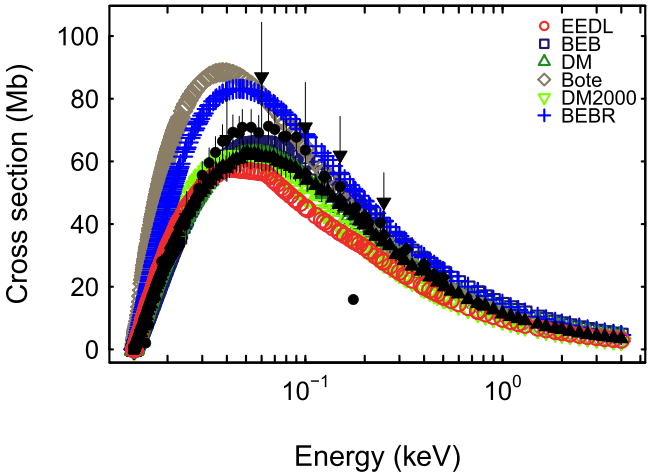

Fig. 8. K shell ionization cross sections for hydrogen ($Z = 1$): experimental data (black and grey filled markers) and cross section models (empty symbols as indicated in the legend).

the relation between ionization and X-ray production cross section for the K shell involves a single atomic parameter, i.e. the fluorescence yield ω_K, while the larger number of parameters relating ionization and X-ray production cross sections for outer shells would complicate the identification of possible systematic effects.

For this purpose the whole analysis chain is repeated with cross sections data recalculated from experimental X-ray production cross sections via equation (1), using the fluorescence yields reported in each of the compilations listed in Table VII; this operation is necessarily limited to the data for which the fluorescence yields originally used by the experimental authors are documented in the respective publications. The presence of systematic effects is assessed by means of categorical data tests, as in the previous analysis stage, which evaluate whether there are any statistically significant differences in the results obtained with different sources of fluorescence yields.

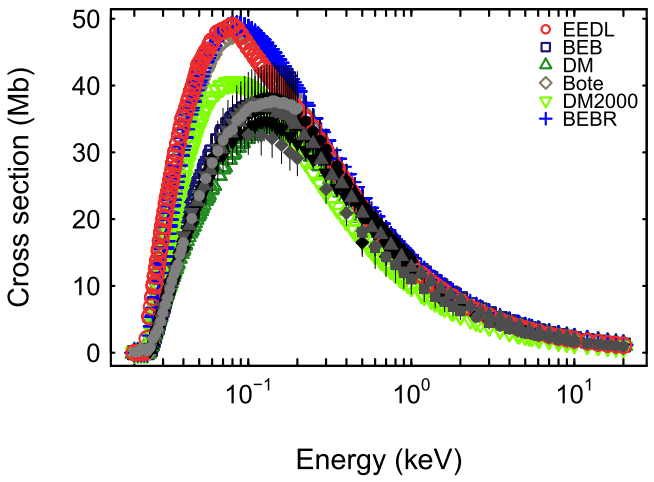

Fig. 9. K shell ionization cross sections for helium ($Z = 2$): experimental data (black and grey filled markers) and cross section models (empty symbols as indicated in the legend).

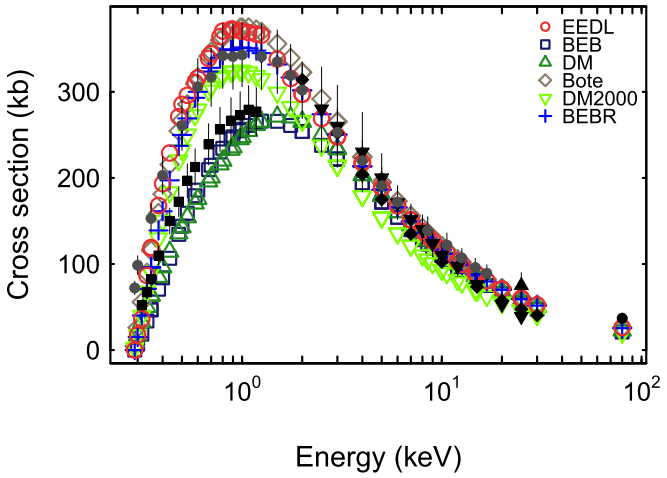

Fig. 10. K shell ionization cross sections for carbon ($Z = 6$): experimental data (black and grey filled markers) and cross section models (empty symbols as indicated in the legend).

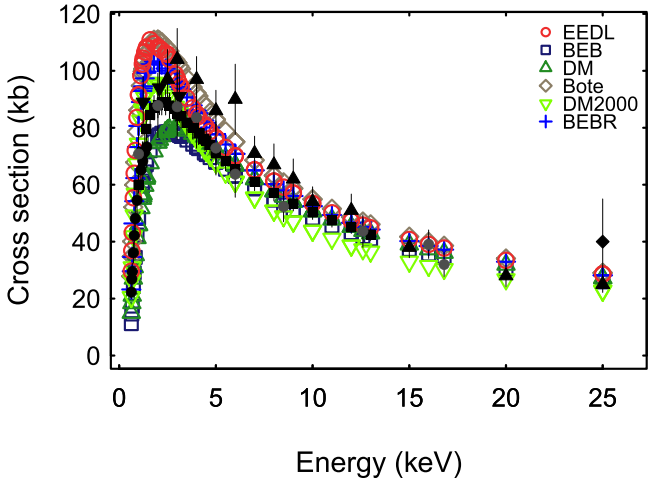

Fig. 11. K shell ionization cross sections for oxygen ($Z = 8$): experimental data (black and grey filled markers) and cross section models (empty symbols as indicated in the legend).

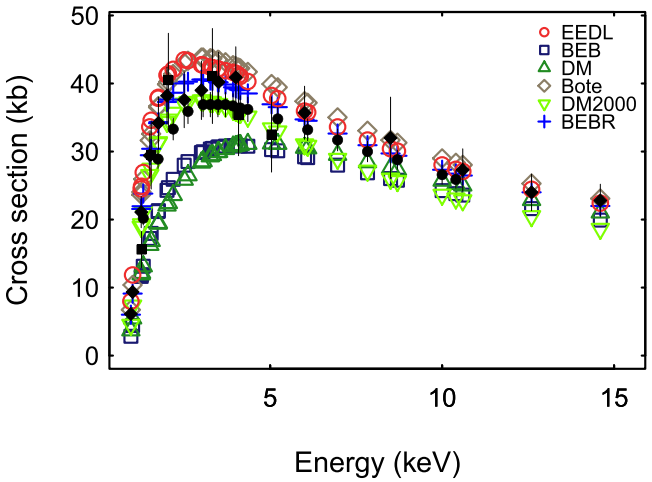

Fig. 12. K shell ionization cross sections for neon ($Z = 10$): experimental data (black and grey filled markers) and cross section models (empty symbols as indicated in the legend).

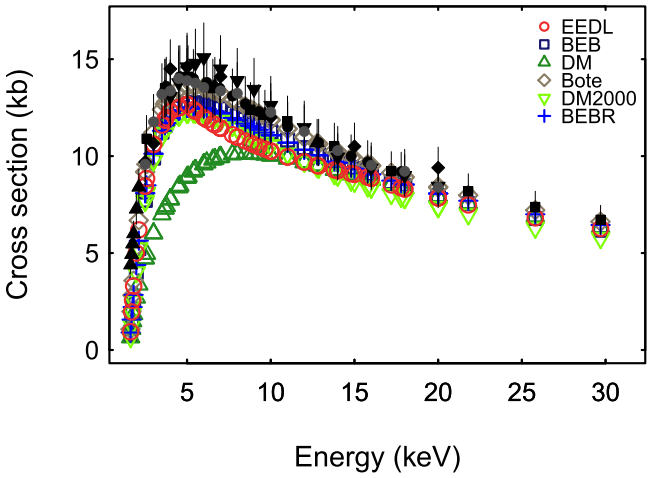

Fig. 13. K shell ionization cross sections for aluminium ($Z = 13$): experimental data (black and grey filled markers) and cross section models (empty symbols as indicated in the legend).

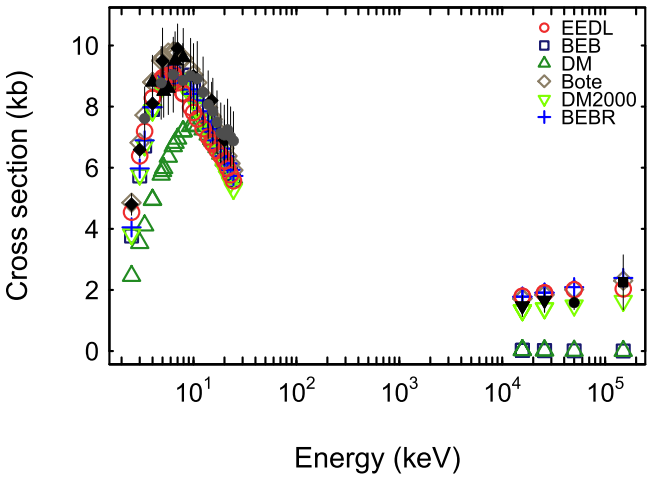

Fig. 14. K shell ionization cross sections for silicon ($Z = 14$): experimental data (black and grey filled markers) and cross section models (empty symbols as indicated in the legend).

The R system [190] (version 3.4.4) and the Statistical Toolkit [191], [192] are used in the data analysis.

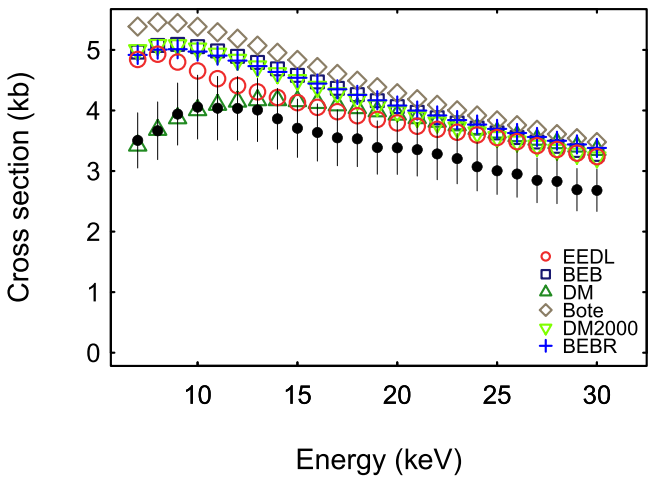

Fig. 15. K shell ionization cross sections for sulfur ($Z = 16$): experimental data (black and grey filled markers) and cross section models (empty symbols as indicated in the legend).

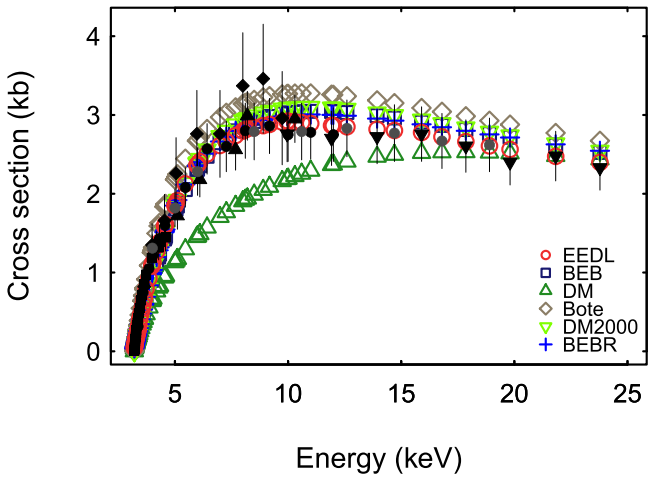

Fig. 16. K shell ionization cross sections for argon ($Z = 18$): experimental data (black and grey filled markers) and cross section models (empty symbols as indicated in the legend).

Further details about the data analysis method are documented in previous publications concerning validation tests, e.g. [193], [194].

VI. Results

The various aspects addressed in the data analysis are detailed in the following sections.

The performance of goodness-of-fit tests to compare calculated and measured cross sections is evaluated in Section VI-A to identify possible sources of systematic effects in the validation process related to specific characteristics of the tests.

The different compatibility with experimental data associated with variants of the analytical formulations or tabulations of the cross section models is discussed in Section VI-B. The outcome of this evaluation is the identification of a subset of cross section models that best represent each modeling approach, over which in-depth analysis is carried out.

The physics results of the validation process concerning the K, L and M shell are reported in Sections VI-C, VI-D, VI-E,

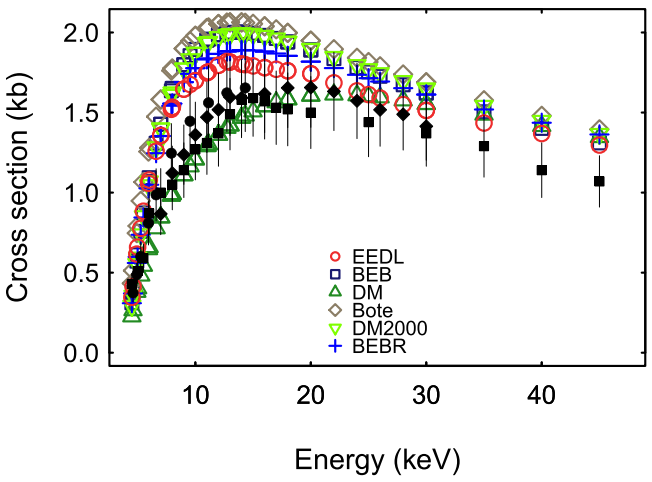

Fig. 17. K shell ionization cross sections for calcium ($Z = 20$): experimental data (black and grey filled markers) and cross section models (empty symbols as indicated in the legend).

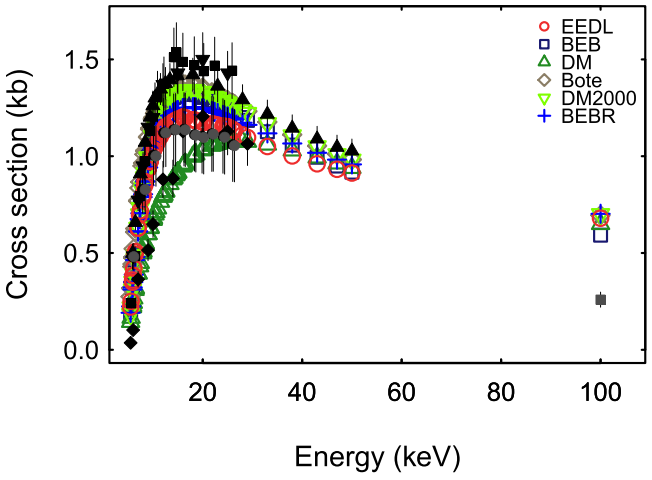

Fig. 18. K shell ionization cross sections for titanium ($Z = 22$): experimental data (black and grey filled markers) and cross section models (empty symbols as indicated in the legend).

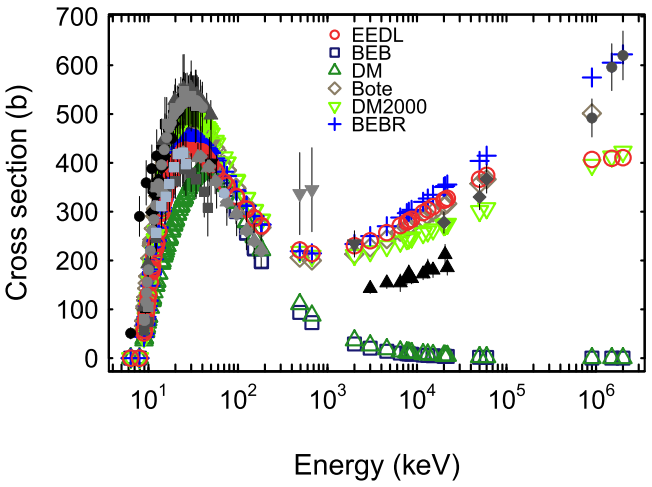

Fig. 19. K shell ionization cross sections for nickel ($Z = 28$): experimental data (black and grey filled markers) and cross section models (empty symbols as indicated in the legend).

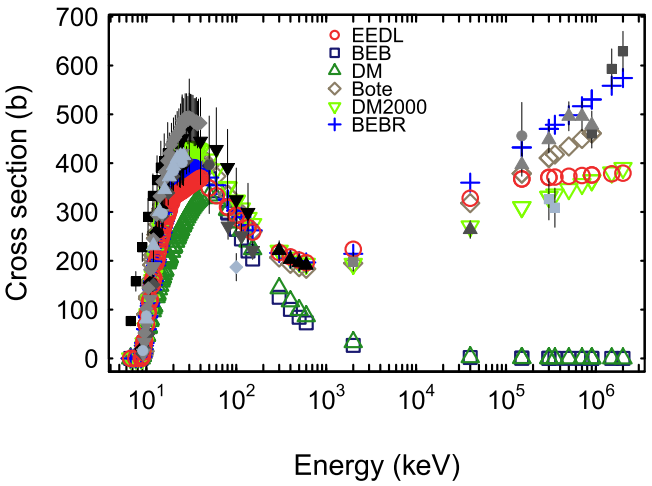

Fig. 20. K shell ionization cross sections for copper ($Z = 29$): experimental data (black and grey filled markers) and cross section models (empty symbols as indicated in the legend).

respectively. They supersede preliminary results presented at conferences [195].

Finally, the investigation of possible systematic effects related to fluorescence yields is discussed in Section VI-F.

A. Choice of Goodness-of-Fit Tests

The effects of applying different goodness-of-fit tests are illustrated in Fig. 1 for the K shell and in Fig. 2 for the L subshells. Although these plots concern a selection of representative cross section calculation methods (EEDL, BEB, DM and Bote) in the energy range between 1 keV and 1 MeV, the following considerations can be generalized to the other models and energies examined in the validation process.

The tests based on the empirical distribution function (Anderson-Darling, Cramer-von-Mises and Kolmogorov-Smirnov) yield consistent results; therefore, only one of them (Anderson-Darling) is retained in the following steps of the analysis.

In general, the χ^2 test rejects the hypothesis of compatibility between calculated and experimental cross sections in a larger fraction of test cases; nevertheless, in this analysis scenario it is not possible to ascertain whether the lower efficiencies associated with the χ^2 test could be a consequence of different statistical power of this test or an artifact of underestimated experimental uncertainties, as discussed in Section III, or a combination of both.

Given the observed differences between the results of the χ^2 and Anderson-Darling tests, categorical data analysis is performed on the basis of the outcome of both tests.

B. Model Variants

1) EEDL Versions: Cross section calculations based on different EEDL data library versions and interpolation methods considered in the validation process yield statistically consistent results in the tests of compatibility with experiment. An example is illustrated in Fig. 3, which shows the

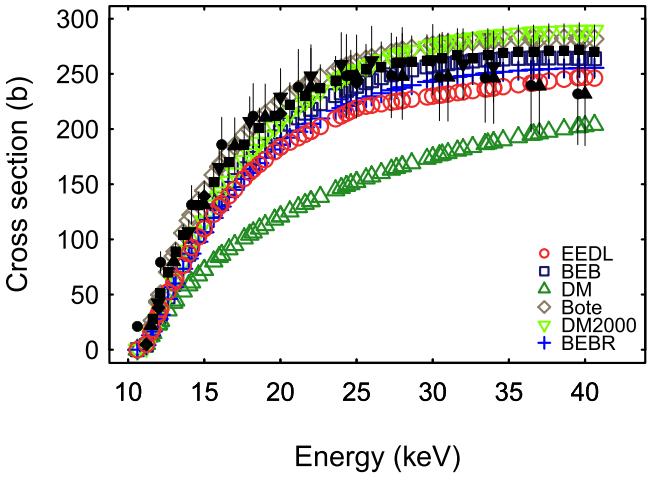

Fig. 21. K shell ionization cross sections for germaium ($Z = 32$): experimental data (black and grey filled markers) and cross section models (empty symbols as indicated in the legend).

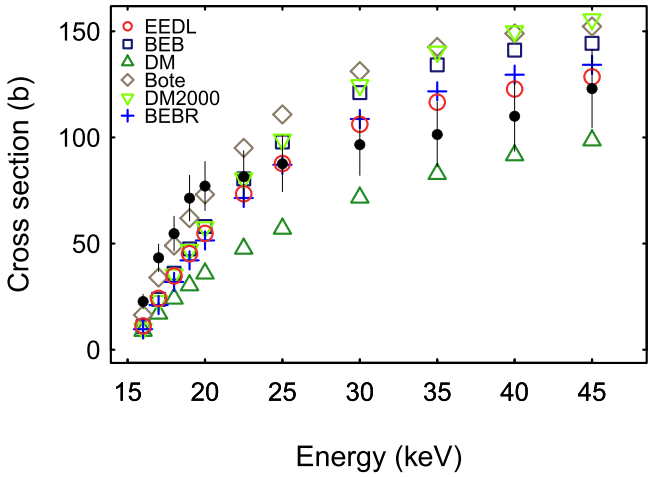

Fig. 23. K shell ionization cross sections for rubidium ($Z = 37$): experimental data (black and grey filled markers) and cross section models (empty symbols as indicated in the legend).

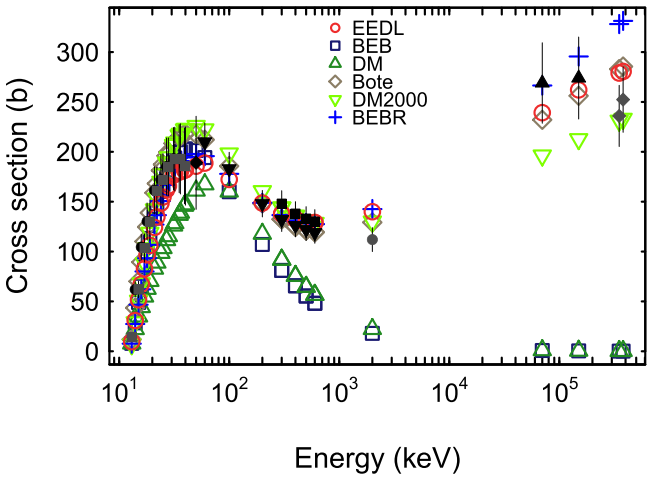

Fig. 22. K shell ionization cross sections for selenium ($Z = 34$): experimental data (black and grey filled markers) and cross section models (empty symbols as indicated in the legend).

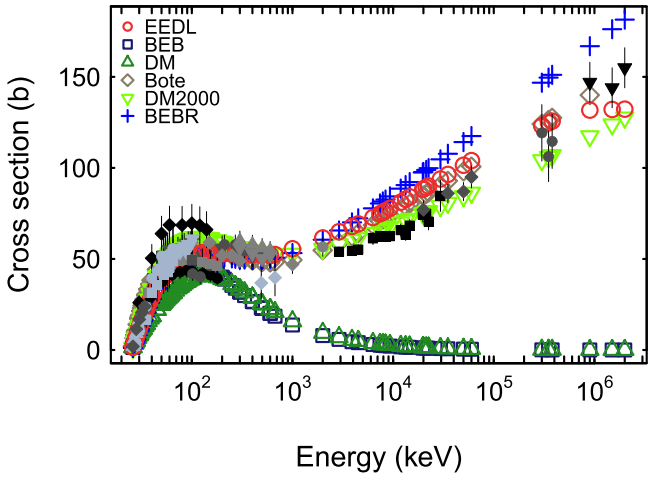

Fig. 24. K shell ionization cross sections for silver ($Z = 47$): experimental data (black and grey filled markers) and cross section models (empty symbols as indicated in the legend).

efficiencies derived from the Anderson-Darling test using the original EEDL released in 1991, the modified EEDL used in Geant4 and the EEDL included in EPICS2017 released in January 2018. The EPICS2017 tabulations are interpolated logarithmically and linearly: the latter interpolation method is recommended in [23] assuming that the number of tabulated data has been extended with respect to the 1991 version, but the size of the tabulations is actually the same as in the original EEDL, for which logarithmic interpolation was recommended.

The apparent lack of sensitivity of the efficiency to the interpolation method of EPICS2017 is linked to the characteristics of the experimental data as well as to features of EEDL tabulations. Inadequate granularity appears to be an issue in all EEDL versions: for example, an effect is visible in Fig. 4, where the cross sections interpolated between approximately 15 and 30 keV exhibit an apparently linear behaviour. It is worth noting that the same interpolation algorithm is applied to Bote tabulations, which are tabulated with higher granularity.

2) Variants of Bote and Salvat Tabulated Cross Sections: Cross sections based on different tabulations derived from Bote and Salvat's calculations produce statistically consistent results in the comparisons with experimental data, although the efficiencies based on Penelope 2014 tabulations are generally larger than those obtained from NIST Standard Database 164. An example is illustrated in Fig. 5, which shows the efficiencies resulting from the χ^2 test. Therefore the subsequent steps of the analysis are limited to Penelope 2014 tabulations.

3) Formulations of the Binary-Encounter-Bethe Model: The efficiency of the formulations of the Binary-Encounter-Bethe documented in Section II-C is summarized in Fig. 6 for the K shell.

The relativistic version of the model exhibits better consistency with experiment at higher energies, as expected. This qualitative observation is confirmed by categorical data analysis for the K and L shell data above 1 MeV, with the rejection of the hypothesis of equivalent compatibility with

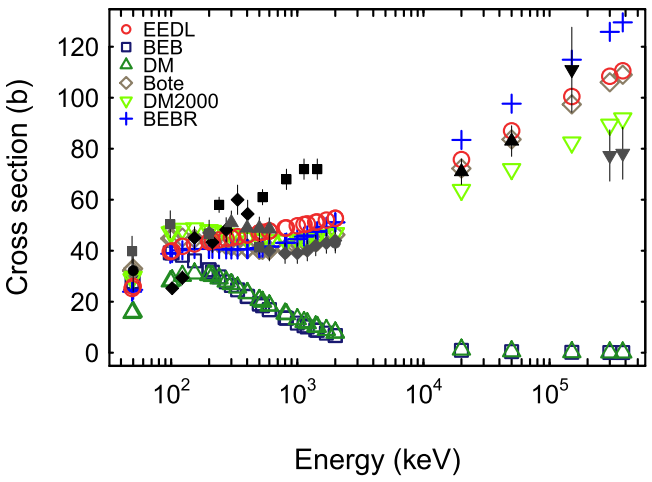

Fig. 25. K shell ionization cross sections for tin ($Z = 50$): experimental data (black and grey filled markers) and cross section models (empty symbols as indicated in the legend).

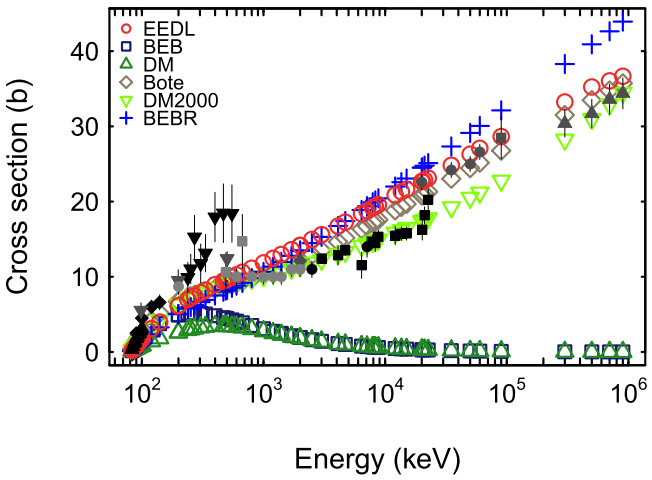

Fig. 26. K shell ionization cross sections for gold ($Z = 79$): experimental data (black and grey filled markers) and cross section models (empty symbols as indicated in the legend).

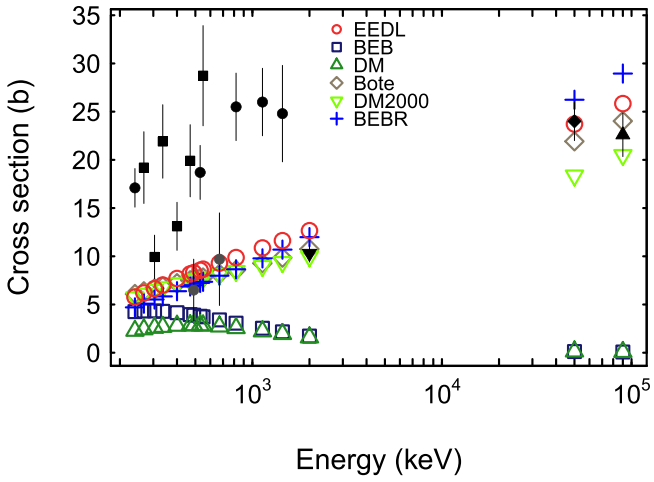

Fig. 27. K shell ionization cross sections for lead ($Z = 82$): experimental data (black and grey filled markers) and cross section models (empty symbols as indicated in the legend).

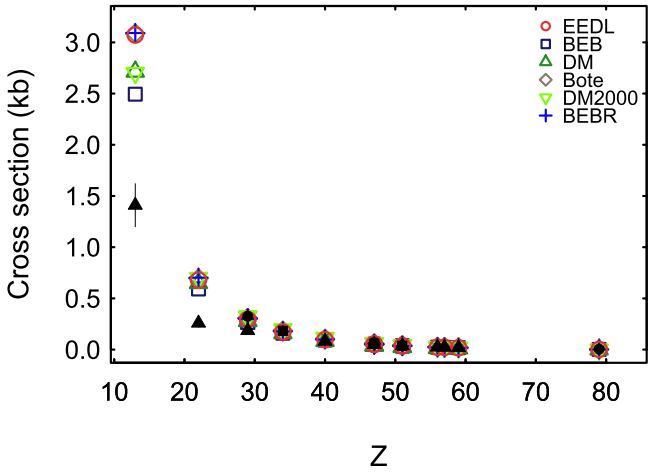

Fig. 28. K shell ionization cross sections as a function of the atomic number for 100 keV electrons: experimental data (black and grey filled markers) and cross section models (empty symbols as indicated in the legend).

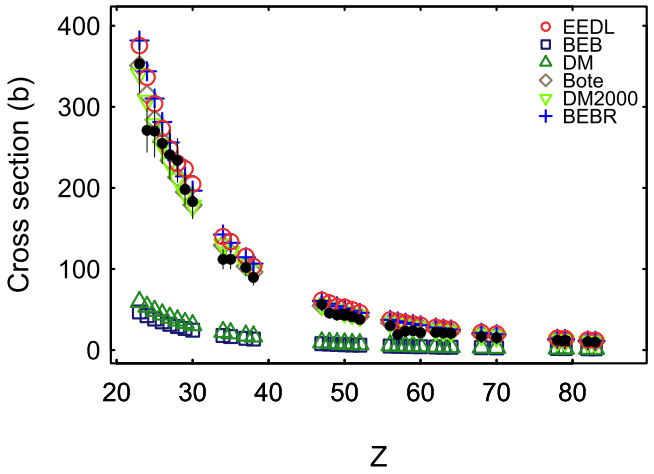

Fig. 29. K shell ionization cross sections as a function of the atomic number for 2 MeV electrons: experimental data (black and grey filled markers) and cross section models (empty symbols as indicated in the legend).

experiment for the relativistic and the original formulation of the model with 0.001 significance. Statistical analysis for individual L subshells would not be meaningful due to the scarcity of experimental data.

The original BEB model is better at describing experimental data at lower energies, while no significant differences are observed at intermediate energies between the original and the relativistic version of the model regarding their compatibility with measurements.

4) Formulations of the Deutsch-Märk Model: The formulations of the Deutsch-Märk model documented in Section II-D exhibit differences in their compatibility with experiment. Fig. 7 summarizes their behaviour for the K shell, reporting the results of comparisons with experimental data derived from the Anderson-Darling goodness-of-fit test.

The earlier version of the model appears to describe experimental K shell cross sections better than the most recent version documented in the literature at the time of writing this paper. All the tests over the corresponding contingency tables for the K shell confirm that the difference in

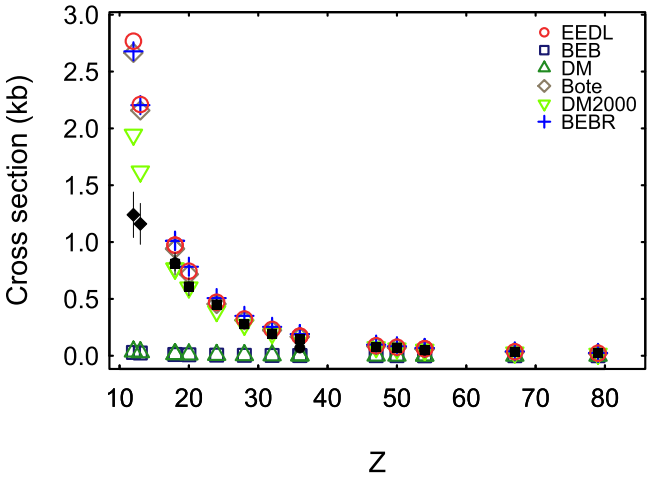

Fig. 30. K shell ionization cross sections as a function of the atomic number for 20 MeV electrons: experimental data (black and grey filled markers) and cross section models (empty symbols as indicated in the legend).

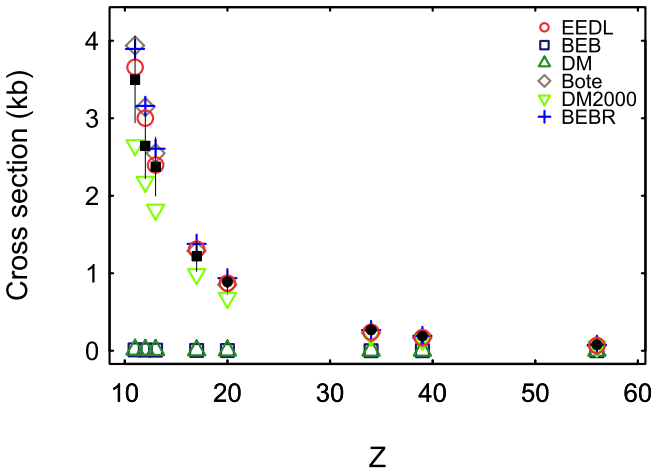

Fig. 32. K shell ionization cross sections as a function of the atomic number for 70 MeV electrons: experimental data (black and grey filled markers) and cross section models (empty symbols as indicated in the legend).

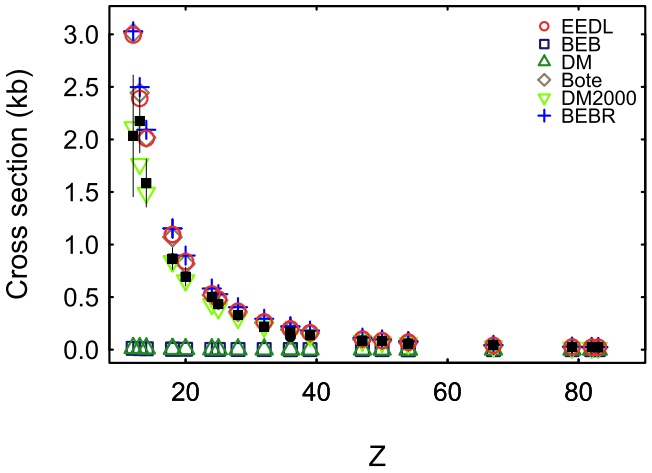

Fig. 31. K shell ionization cross sections as a function of the atomic number for 50 MeV electrons: experimental data (black and grey filled markers) and cross section models (empty symbols as indicated in the legend).

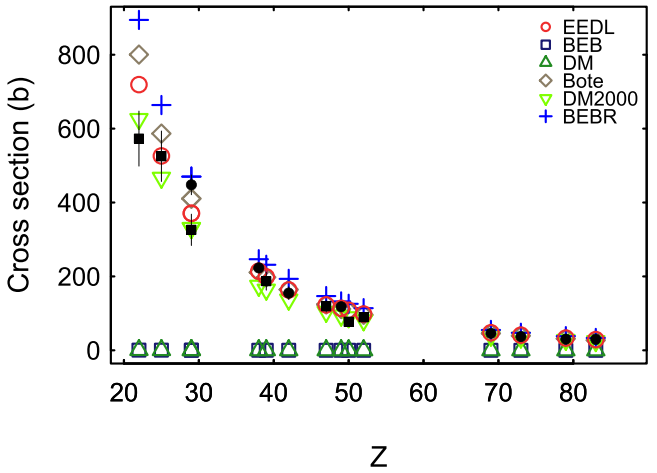

Fig. 33. K shell ionization cross sections as a function of the atomic number for 300 MeV electrons: experimental data (black and grey filled markers) and cross section models (empty symbols as indicated in the legend).

compatibility with experiment between the two versions of the Deutsch-Märk model is statistically significant, resulting in p-values smaller than 0.001, with the exception of the energy range below 1 keV, where the hypothesis of equivalent compatibility with measurements is not rejected with 0.01 significance. No statistically significant difference is observed in the analysis of the contingency tables for the L subshells.

The relativistic version of the model exhibits better consistency with experiment at higher energies, as expected; nevertheless, above 1 MeV the difference in compatibility with experimental data with respect to the earlier version is not statistically significant.

C. K Shell

A selection of experimental and calculated K shell ionization cross sections is illustrated in Figs. 8–33. The purpose of these figures, as well of the following ones concerning L and M shell ionization cross sections, is to illustrate qualitatively the problem domain: they address the general features rather than the details of the models and of the experimental measurements, providing an overview of the characteristics of the data involved in the validation process. They are not intended as an instrument to evaluate the agreement or disagreement between models and experimental data: this is the task of the statistical analysis.

The efficiencies resulting from the tests comparing calculated and experimental K shell cross sections are listed in Table VIII along with the number of test cases from which they derive. The results are reported for two energy ranges: starting from 100 eV and from 1 keV. The latter corresponds to the domain of applicability of most general purpose Monte Carlo transport codes; the former is the limit of use of EEDL recommended in [23], which is reflected on the Monte Carlo codes that use this evaluated data library as the basis for electron transport.

The p-values resulting from categorical data analysis based on the outcome of goodness-of-fit tests are reported in Table IX, for electron energies equal or above 100 eV.

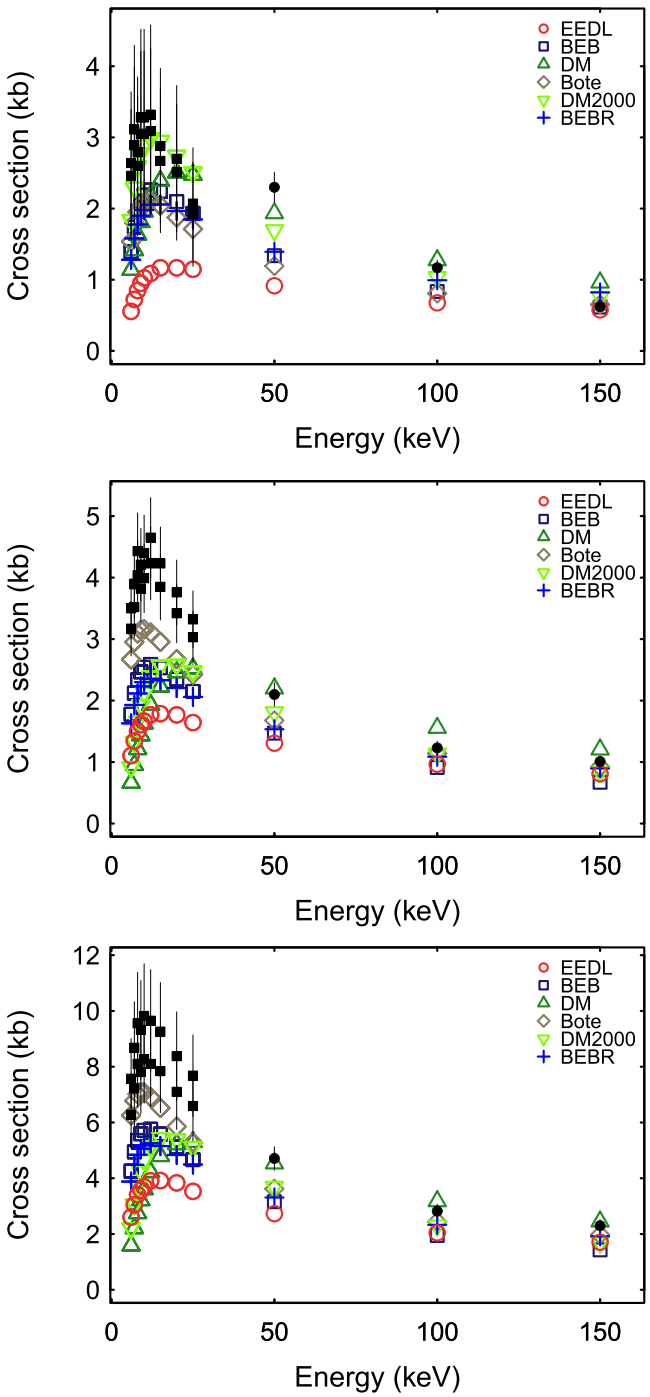

Fig. 34. L subshell ionization cross sections for silver ($Z = 47$): experimental data (black and grey filled markers) and cross section models (empty symbols as indicated in the legend): L_1 (top), L_2 (middle) and L_3 (bottom) subshells.

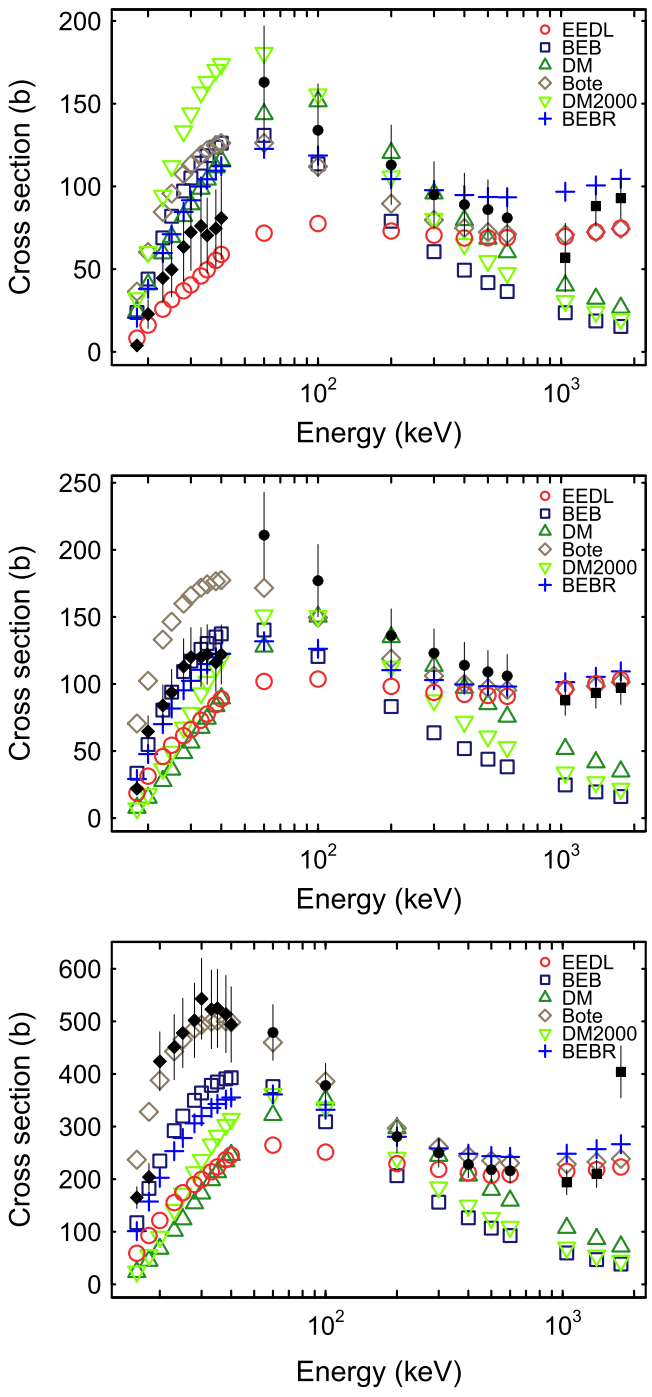

Fig. 35. L subshell ionization cross sections for lead ($Z = 82$): experimental data (black and grey filled markers) and cross section models (empty symbols as indicated in the legend): L_1 (top), L_2 (middle) and L_3 (bottom) subshells.

They concern the comparison of the compatibility with experiment of the Bote model, evaluated by two goodness-of-fit tests (χ^2 and Anderson-Darling), with that of the other models.

The null hypothesis of equivalent compatibility with experiment between Bote and other models is not rejected by any of the tests applied to the respective contingency tables. The same conclusion is reached by using the outcome of the χ^2 and Anderson-Darling tests as input to the categorical data analysis: this means that, even if the two goodness-of-fit tests produce different results in the comparison of calculated and measured K shell cross sections, as is discussed in Section VI-A, the identification of the state of the art in cross section modeling is not affected by the choice of the goodness-of-fit test used to determine the incompatibility between calculations and experiment. The same conclusion also holds for the Cramer-von Mises and Kolmogorov-Smirnov tests, whose results are not reported in detail here.

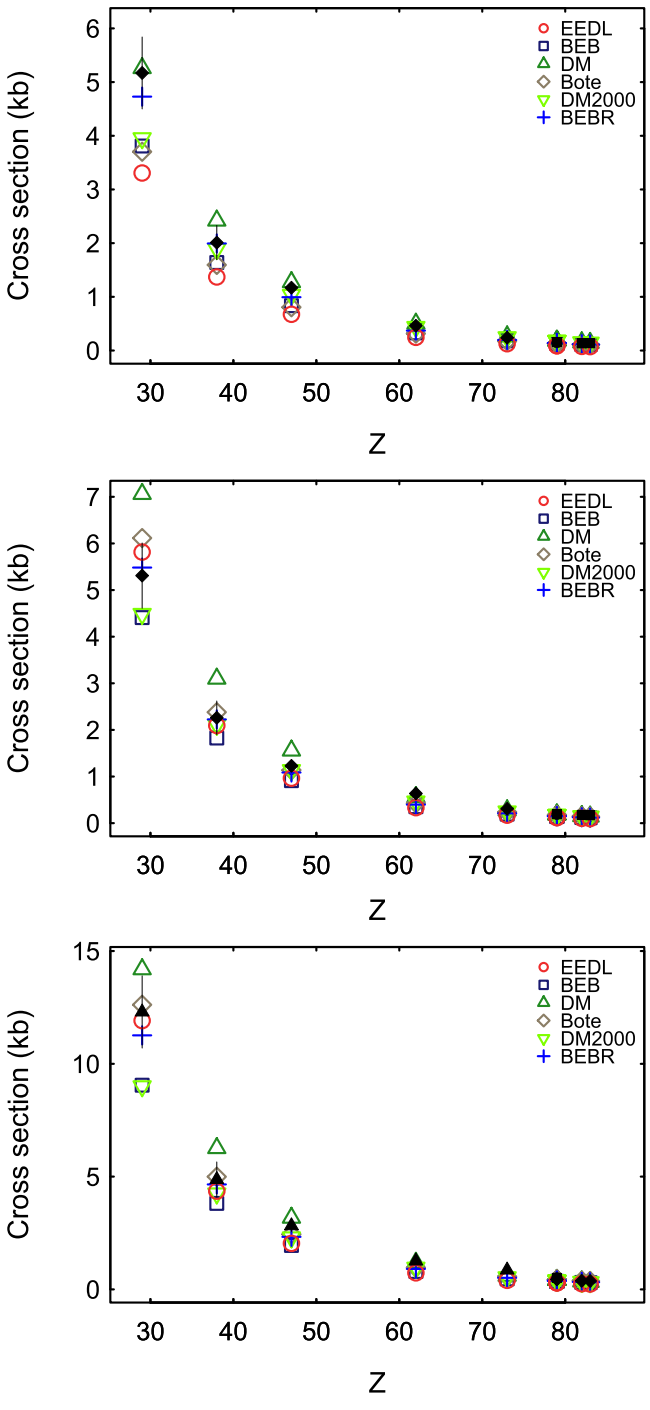

Fig. 36. L subshell ionization cross sections at 100 keV as a function of the atomic number: experimental data (black and grey filled markers) and cross section models (empty symbols as indicated in the legend): L_1 (top), L_2 (middle) and L_3 (bottom) subshells.

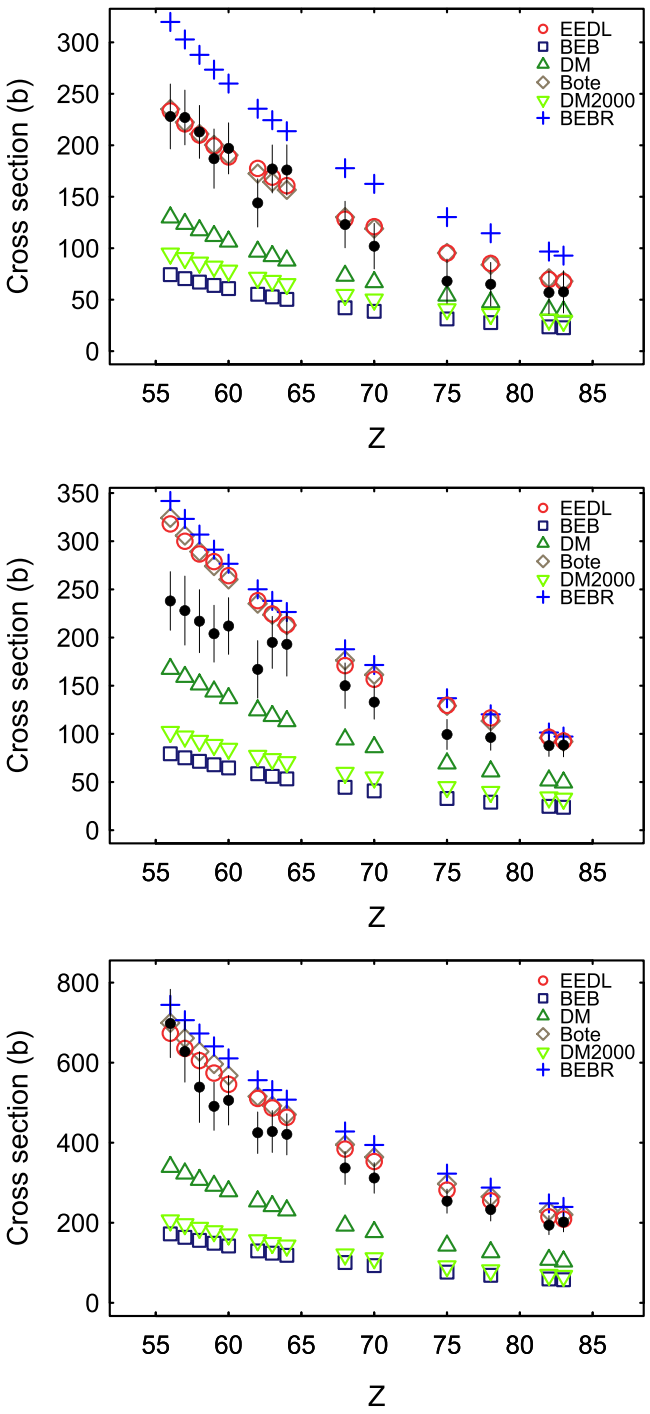

Fig. 37. L subshell ionization cross sections at 1.04 MeV as a function of the atomic number: experimental data (black and grey filled markers) and cross section models (empty symbols as indicated in the legend): L_1 (top), L_2 (middle) and L_3 (bottom) subshells.

The analysis for electron energies equal or above 1 keV leads to the same conclusions.

D. L Shell

A selection of experimental and calculated L subshell ionization cross sections is illustrated in Figs. 34–39.

The validation process concerns the calculation of cross sections for the L_1, L_2 and L_3 subshells, which are the quantities of interest for Monte Carlo transport codes; since the experimental data sample for the single subshells is relatively small, the results are also reported collectively for the whole L shell. Nevertheless, even grouping the data the number of tests cases in the validation of L shell cross sections remains substantially smaller than in the analysis for the K shell. The tests encompass the whole energy range covered by the experimental data.

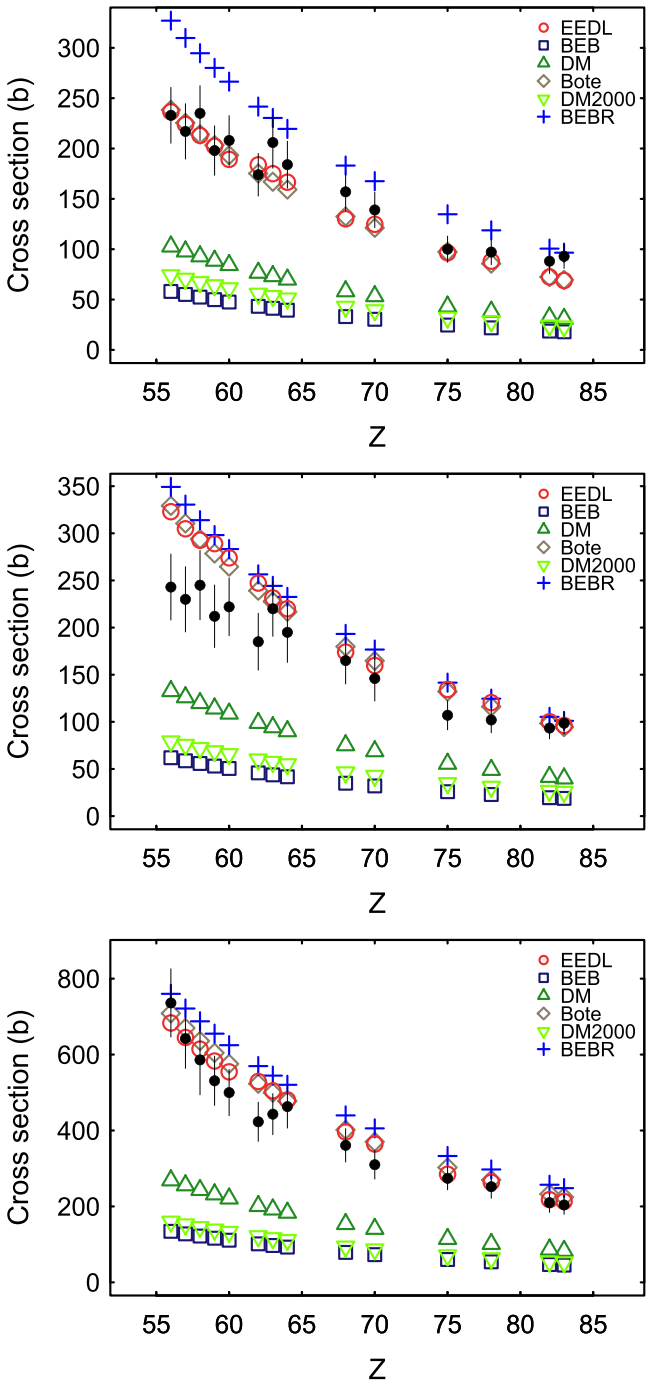

Fig. 38. L subshell ionization cross sections at 1.39 MeV as a function of the atomic number: experimental data (black and grey filled markers) and cross section models (empty symbols as indicated in the legend): L_1 (top), L_2 (middle) and L_3 (bottom) subshells.

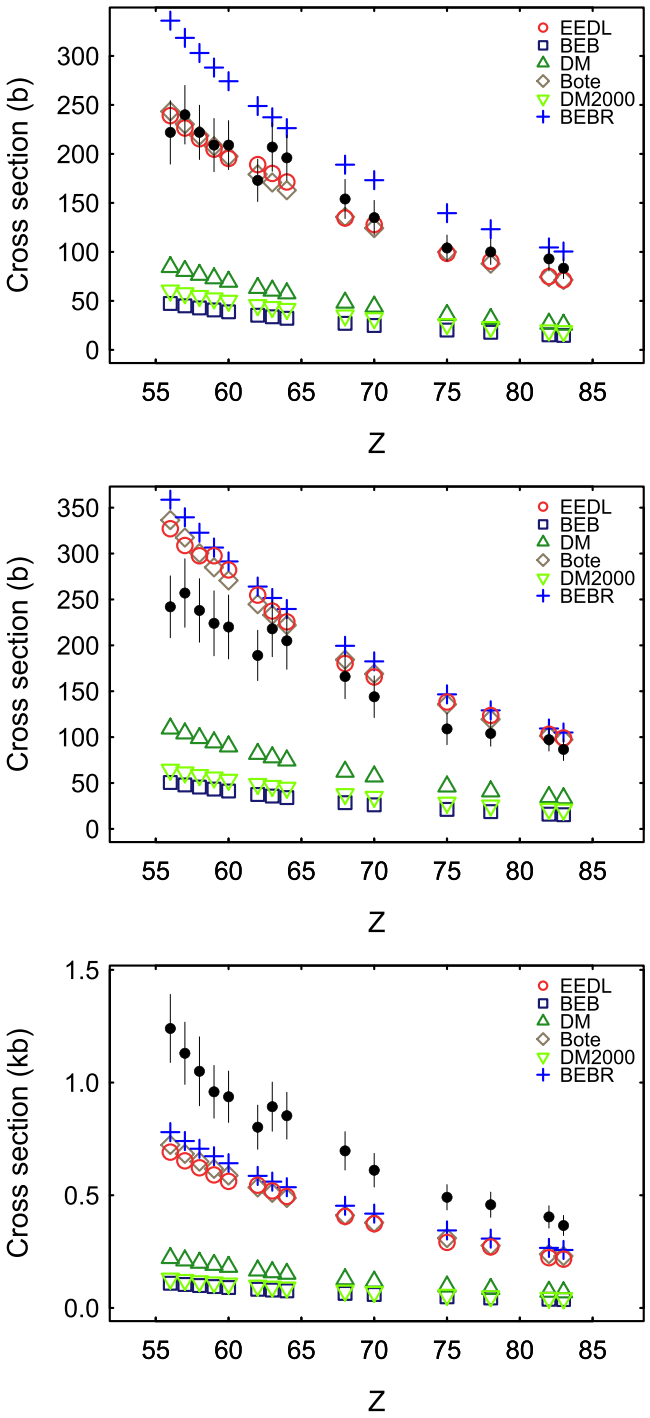

Fig. 39. L subshell ionization cross sections at 1.76 MeV as a function of the atomic number: experimental data (black and grey filled markers) and cross section models (empty symbols as indicated in the legend): L_1 (top), L_2 (middle) and L_3 (bottom) subshells.

The efficiencies resulting from the goodness-of-fit tests comparing calculated and experimental L subshell cross sections are listed in Table X along with the number of test cases on which they are based.

The results of the categorical data analysis based on the outcome of the χ^2 and Anderson-Darling goodness-of-fit tests are summarized in Table XI.

The hypothesis of equivalent compatibility with experiment for EEDL and Bote cross sections is not rejected for the L_1 and L_2 subshells. The results regarding the L_3 subshell and the grouped L shell data are somewhat controversial: the null hypothesis is not rejected on the basis of the outcome of the Anderson-Darling test, while it is rejected on the basis of the outcome of the χ^2 goodness-of-fit test by all the tests applied to the contingency tables, with the exception of Fisher's exact test, which is known to be more conservative over 2×2 tables [196].

TABLE VIII

EFFICIENCIES RESULTING FROM THE χ^2 AND ANDERSON-DARLING TESTS FOR THE K SHELL

Energy	Model	χ^2	Anderson-Darling
≥100 eV (173 test cases)	EEDL	0.68 ± 0.04	0.73 ± 0.03
	Bote	0.68 ± 0.04	0.80 ± 0.03
	BEBR	0.55 ± 0.04	0.73 ± 0.03
	DM2000	0.64 ± 0.04	0.83 ± 0.03
≥1 keV (167 test cases)	EEDL	0.72 ± 0.03	0.75 ± 0.04
	Bote	0.71 ± 0.03	0.81 ± 0.03
	BEBR	0.59 ± 0.04	0.74 ± 0.04
	DM2000	0.66 ± 0.04	0.82 ± 0.03

TABLE IX

P-VALUES OF TESTS OVER CONTINGENCY TABLES COMPARING THE COMPATIBILITY WITH EXPERIMENT OF BOTE MODEL WITH THAT OF OTHER MODELS, K SHELL

GoF test	Model	Fisher	Pearson χ^2	Z-pooled	Boschloo	CSM
χ^2	EEDL	1.000	1.000	1.000	1.000	0.999
	BEBR	0.020	0.015	0.015	0.015	0.015
	DM2000	0.495	0.426	0.532	0.443	0.475
AD	EEDL	0.238	0.190	0.246	0.201	0.281
	BEBR	0.192	0.151	0.165	0.165	0.233
	DM2000	0.570	0.477	0.522	0.519	1.000

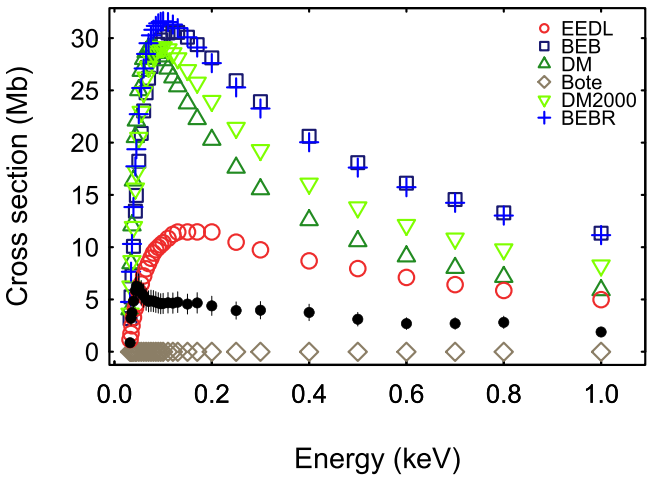

Fig. 40. M_1 subshell ionization cross sections for argon ($Z = 18$): experimental data (black filled markers) and cross section models (empty symbols as indicated in the legend).

The hypothesis of equivalent compatibility with experiment between Bote and relativistic Binary-Encounter-Bethe cross sections is not rejected for any of the test configurations considered in the analysis. The results concerning the earlier version of the Deutsch-Märk model appear similar to those previously discussed regarding the comparison of the capabilities of EEDL and Bote cross sections.

Caution should be exercised in drawing conclusions from these results, as the rejection of the null hypothesis of compatibility between calculated and experimental cross sections in the χ^2 test could be biased in some cases by underestimated experimental uncertainties, which are explicitly involved in the calculation of the χ^2 test statistic. The scarcity of experimental data for the L shell prevents a thorough investigation of the reported experimental errors and of the possible presence of systematic effects, which is feasible only when an extensive data sample allows a critical assessment of measurements reported by different experiments.

TABLE X

EFFICIENCIES RESULTING FROM THE χ^2 AND ANDERSON-DARLING TESTS FOR THE L SHELL

Shell	Model	χ^2	Anderson-Darling
L_1 (17 test cases)	EEDL	0.53 ± 0.11	0.63 ± 0.11
	Bote	0.59 ± 0.11	0.75 ± 0.10
	BEBR	0.47 ± 0.11	0.88 ± 0.09
	DM2000	0.53 ± 0.11	0.50 ± 0.11
L_2 (23 test cases)	EEDL	0.30 ± 0.09	0.55 ± 0.10
	Bote	0.48 ± 0.10	0.77 ± 0.09
	BEBR	0.52 ± 0.10	0.86 ± 0.07
	DM2000	0.17 ± 0.08	0.77 ± 0.09
L_3 (25 test cases)	EEDL	0.24 ± 0.08	0.58 ± 0.10
	Bote	0.64 ± 0.09	0.88 ± 0.07
	BEBR	0.36 ± 0.09	0.79 ± 0.08
	DM2000	0.08 ± 0.06	0.54 ± 0.10
L (65 test cases)	EEDL	0.34 ± 0.06	0.58 ± 0.06
	Bote	0.57 ± 0.06	0.81 ± 0.05
	BEBR	0.45 ± 0.06	0.84 ± 0.05
	DM2000	0.23 ± 0.05	0.61 ± 0.06

TABLE XI

P-VALUES OF TESTS OVER CONTINGENCY TABLES COMPARING THE COMPATIBILITY WITH EXPERIMENT OF BOTE MODEL WITH THAT OF OTHER MODELS, L SHELL

Shell	GoF test	Model	Fisher	Pearson χ^2	Z-pooled	Boschloo	CSM
L_1	χ^2	EEDL	1.000	0.730	0.848	1.000	0.964
		BEBR	0.732	0.492	0.608	0.608	0.941
		DM2000	1.000	0.730	0.848	1.000	0.964
	AD	EEDL	0.704	-	0.527	0.514	0.455
		BEBR	0.654	-	0.527	0.424	0.646
		DM2000	0.273	-	0.227	0.169	0.163
L_2	χ^2	EEDL	0.365	0.227	0.259	0.258	0.182
		BEBR	1.000	0.768	0.883	1.000	0.996
		DM2000	0.057	-	0.030	0.030	0.029
	AD	EEDL	0.203	0.112	0.125	0.125	0.123
		BEBR	0.698	-	0.529	0.489	0.878
		DM2000	1.000	1.000	1.000	1.000	0.943
L_3	χ^2	EEDL	0.010	0.004	0.005	0.005	0.005
		BEBR	0.089	0.048	0.065	0.065	0.094
		DM2000	<0.001	-	<0.001	<0.001	<0.001
	AD	EEDL	0.049	-	0.029	0.029	0.025
		BEBR	0.701	-	0.529	0.492	0.945
		DM2000	0.024	-	0.013	0.013	0.012
L	χ^2	EEDL	0.013	0.008	0.009	0.009	0.009
		BEBR	0.219	0.160	0.210	0.188	0.397
		DM2000	<0.001	<0.001	<0.001	<0.001	<0.001
	AD	EEDL	0.011	0.006	0.007	0.007	0.007
		BEBR	0.815	0.638	0.685	0.685	1.000
		DM2000	0.029	0.018	0.018	0.019	0.020

E. M Shell

The extreme scarcity of experimental data for M subshells prevents a proper statistical analysis for the validation of the various cross section calculation methods. Only a qualitative appraisal of their ability to reproduce experimental

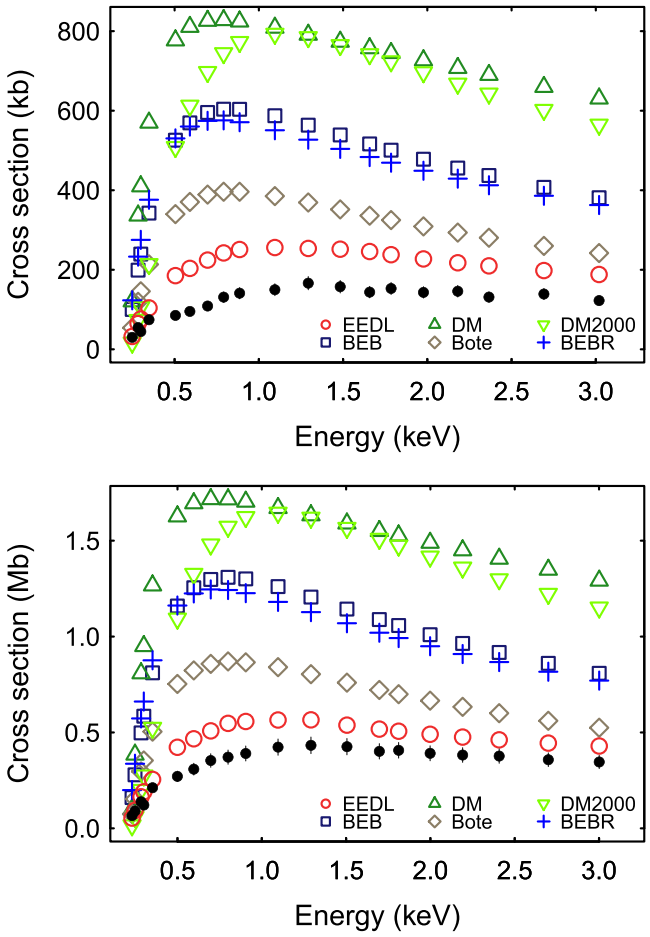

Fig. 41. M subshell ionization cross sections for krypton ($Z = 36$): experimental data (black and grey filled markers) and cross section models (empty symbols as indicated in the legend): M_2 (top) and M_3 (bottom) subshells.

measurements is possible in Figs. 40–43; no general conclusion can be drawn from such an unrepresentative data sample.

F. Influence of Fluorescence Yield Variations

The investigation of possible systematic effects in the validation process due to the values of fluorescence yields used to extract K shell ionization cross sections from measured X-ray production cross sections is summarized in Table XII. The table reports the p-values resulting from Boschloo test over the contingency tables derived from the statistical comparison of calculated and experimental ionization cross sections, where the experimental cross sections have been obtained using the fluorescence yields drawn from the compilations listed in Table VII. The p-values identified as "default" are those corresponding to the original analysis, reported in Table IX.

From these results one can infer that the analysis reaches the same conclusions regarding the hypothesis of equivalent compatibility with experiment of Bote, EEDL and the earlier Deutsch-Märk models, irrespective of the fluorescence yields that are used to determine the experimental cross sections involved in the validation tests. Controversial results are obtained regarding the hypothesis of equivalent capability of

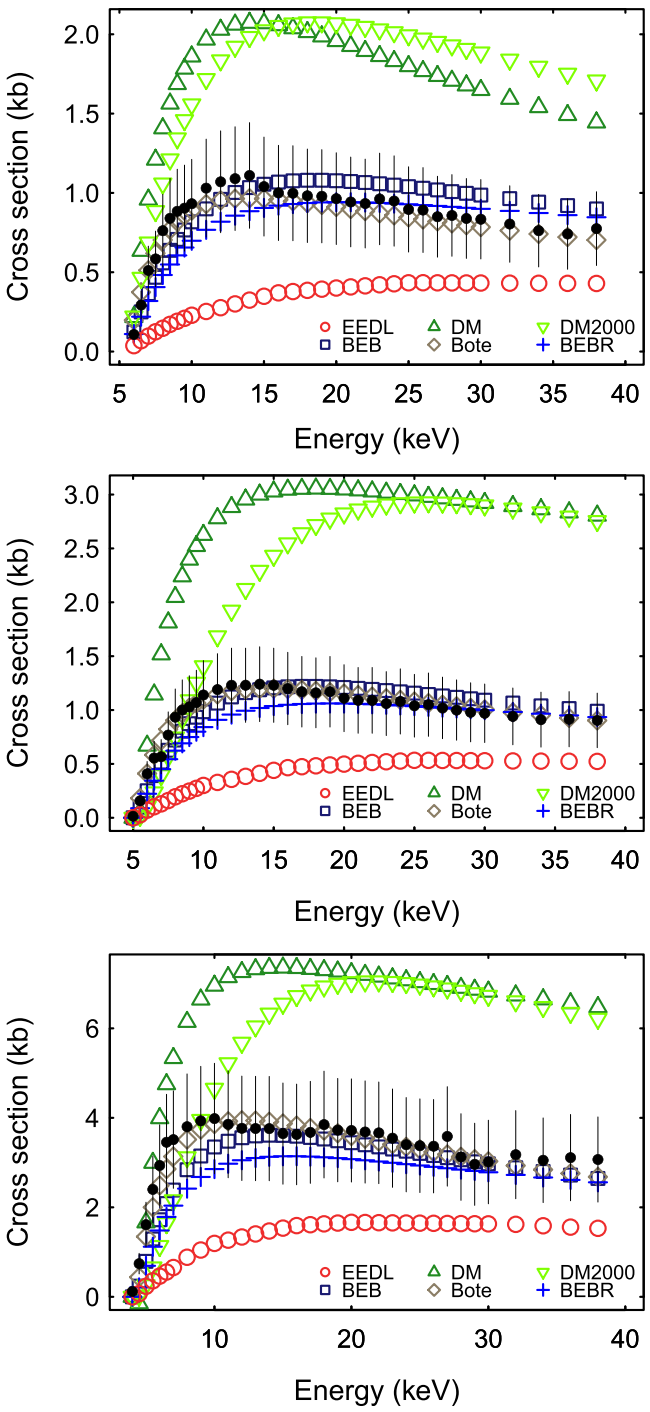

Fig. 42. M subshell ionization cross sections for uranium ($Z = 92$): experimental data (black and grey filled markers) and cross section models (empty symbols as indicated in the legend): M_1 (top), M_2 (middle) and M_3 (bottom) subshells.

Bote and BEBR models to reproduce experimental data: the null hypothesis is rejected or not rejected with 0.01 significance, depending on which fluorescence yields are used, in the analysis of contingency tables based on the outcome of the χ^2 goodness-of-fit test.

It is notable that the null hypothesis is often rejected in association with more modern compilations of fluorescence yields, which benefit from a more extensive experimental

TABLE XII

P-VALUE RESULTING FROM BOSCHLOO TEST COMPARING THE COMPATIBILITY WITH EXPERIMENT OF BOTE MODEL WITH THAT OF OTHER MODELS USING DIFFERENT FLUORESCENCE YIELDS, K SHELL

Test	Model	Default	Bambynek 1972	Bambynek 1984	Krause	Hubbell 1994	Kahoul 2012	Kahoul F_1	Kahoul F_3	Kahoul F_4	Kahoul F_5	Daoudi	EADL	Elam	XOP
χ^2	EEDL	1.000	0.665	1.000	0.855	0.279	0.487	0.058	0.082	0.076	0.200	0.504	0.298	0.302	0.504
	BEBR	0.015	0.021	0.180	0.012	0.004	0.006	<0.001	0.001	<0.001	0.004	0.006	0.003	0.006	0.012
	DM2000	0.443	1.000	0.205	1.000	0.404	0.487	0.045	0.015	0.001	0.015	0.504	0.661	0.579	1.000
AD	EEDL	0.201	0.240	0.316	0.200	0.077	0.361	0.068	0.043	0.029	0.026	0.068	0.068	0.087	0.529
	BEBR	0.165	0.087	0.263	0.122	0.040	0.120	0.026	0.032	0.016	0.036	0.029	0.087	0.036	0.175
	DM2000	0.519	0.818	0.598	0.702	0.503	1.000	0.596	0.444	0.444	0.287	0.709	1.000	0.444	0.517

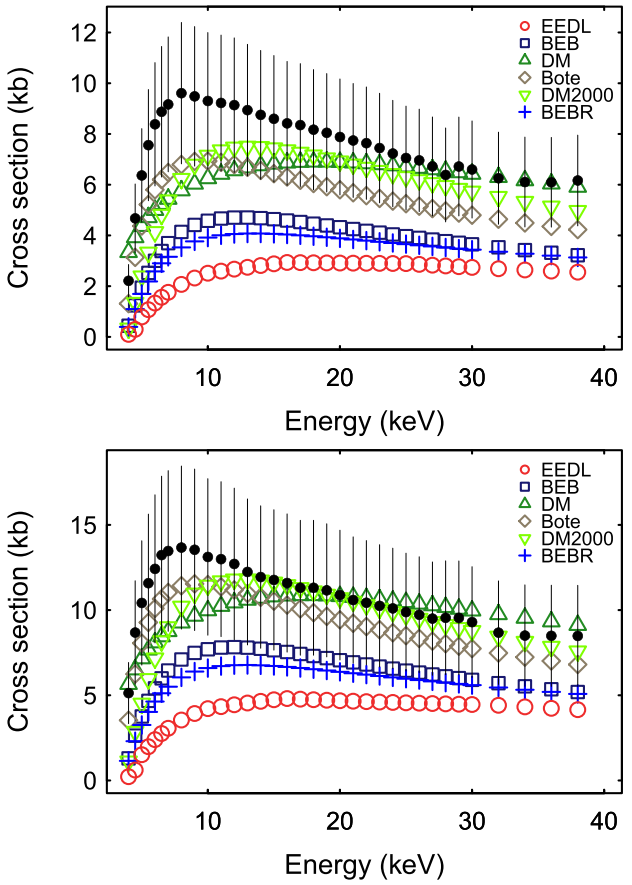

Fig. 43. M subshell ionization cross sections for uranium ($Z = 92$): experimental data (black and grey filled markers) and cross section models (empty symbols as indicated in the legend): M_4 (top), and M_5 (bottom) subshells.

database. It is also worth noting that in some cases where the null hypothesis is not rejected the p-value is close to the critical region; with the exception of the data related to Bambynek1984 compilation, the null hypothesis would be rejected at 0.05 significance level.

Although only the results of Boschloo test are discussed in detail here, similar considerations can also be made on the results of the other tests applied to contingency tables.

This analysis shows that the conclusions of the validation process are robust with respect to the use of different fluorescence yields for the two models of electron impact ionization cross sections currently used in Monte Carlo transport codes, EEDL and Bote, and the Deutsch-Märk model. Nevertheless, it also highlights that the role of these atomic parameters should not be neglected in the determination of ionization cross sections from X-ray production measurements, since they are liable to introduce systematic effects depending on which source is used for their values.

VII. CONCLUSION

The study documented in this paper evaluated several calculation methods for electron impact ionization cross sections with respect to a wide collection of experimental measurements. The results are objectively quantified by means of statistical analysis methods.

All cross section models are available in a variety of formulations and tabulations; statistical validation tests have highlighted their respective strengths and problems. No substantial dissimilarity regarding compatibility with experiment is observed between the cross sections derived from the EEDL version currently used by Monte Carlo codes, dating back to 1991, and those based on the version released in early 2018 within EPICS2017 and ENDF/B-VIII.0. Issues related to inadequate granularity of EEDL tabulations have not been addressed in the new version. No significantly different behaviour with respect to experimental data is observed between the tabulations of Bote and Salvat calculations distributed in Penelope 2014 and in the NIST Database 164. The earlier version of the Deutsch-Märk model performs better than the current one with respect to experimental data for the K shell, while no significant discrepancy in compatibility with experiment between the two versions is observed for the L subshells. No single formulation of the Binary-Encounter-Bethe model can reproduce the experimental measurements documented in the literature over the whole energy range: the original model and its relativistic formulation are suitable for the lower and higher ends, respectively.

The results of the validation process are especially meaningful for K shell ionization cross sections, which are the most interesting in the experimental application context, thanks to the extensive experimental data sample available for validation tests. The statistical analysis has not identified any substantial difference between the capability of EEDL and the more recent calculations by Bote and Salvat to accurately describe K shell ionization cross sections. No significant differences in compatibility with experiment are identified either between

the earlier version of the Deutsch-Märk model and Bote and Salvat calculations.

Possible systematic effects associated with deriving ionization cross sections from measurements of X-ray production cross sections have been studied, considering several compilations of K-shell fluorescence yields. The conclusions concerning EEDL, Bote and Salvat calculations, and the Deutsch-Märk model are robust, i.e. they are insensitive to which fluorescence yields are used in the experimental conversion.

The results concerning L subshells are controversial: the statistical analysis gives some indication of the Bote model as superior to EEDL at reproducing experimental L_3 subshell ionization cross sections, while no significant differences are identified in the analysis concerning the L_1 and L_2 subshells. Moreover, the results concerning the L_3 subshell are not unequivocal, since different goodness-of-fit tests used in the validation process lead to different conclusions. Furthermore, no substantial discrepancy is identified between the capabilities of the relativistic Binary-Encounter-Bethe and Bote models. More measurements of L subshell ionization cross sections, preferably originating from several independent experiments, would be needed to unambiguously discriminate the capabilities of the models.

The very limited availability of experimental M subshell ionization cross sections prevents a meaningful validation analysis.

As a result of the validation process, both EEDL and Bote and Salvat tabulations can be recommended for use in Monte Carlo particle transport.

ACKNOWLEDGMENT

The contribution of the CERN Library has been essential to this study. The authors thank S. Bertolucci and M. Paganoni for their support as CERN Director of Research and Head of the Physics Department at the University of Milano-Bicocca, and A. Hollier for proofreading the manuscript.

REFERENCES

[1] H. Seo, M. G. Pia, P. Saracco, and C. H. Kim, "Ionization cross sections for low energy electron transport," *IEEE Trans. Nucl. Sci.*, vol. 58, no. 6, pp. 3219–3245, Dec. 2011.

[2] S. Guatelli, A. Mantero, B. Mascialino, P. Nieminen, and M. G. Pia, "Geant4 atomic relaxation," *IEEE Trans. Nucl. Sci.*, vol. 54, no. 3, pp. 585–593, Jun. 2007.

[3] S. Guatelli, A. Mantero, B. Mascialino, M. G. Pia, and V. Zampichelli, "Validation of Geant4 atomic relaxation against the NIST physical reference data," *IEEE Trans. Nucl. Sci.*, vol. 54, no. 3, pp. 594–603, Jun. 2007.

[4] H. Deutsch, K. Becker, B. Gstir, and T. D. Märk, "Calculated electron impact cross sections for the K-shell ionization of Fe, Co, Mn, Ti, Zn, Nb, and Mo atoms using the DM formalism," *Int. J. Mass Spectrometry*, vol. 213, no. 1, pp. 5–8, 2002.

[5] X. Llovet, C. J. Powell, F. Salvat, and A. Jablonski, "Cross sections for inner-shell ionization by electron impact," *J. Phys. Chem. Ref. Data*, vol. 43, p. 013102, Jan. 2014.

[6] S. T. Perkins, D. E. Cullen, and S. M. Seltzer, "Tables and graphs of electron-interaction cross sections from 10 eV to 100 GeV derived from the LLNL evaluated data library (EEDL), $Z = 1-100$," Lawrence Livermore Nat. Lab., Tech. Rep. UCRL-50400, 1991, vol. 31.

[7] D. Bote and F. Salvat, "Calculations of inner-shell ionization by electron impact with the distorted-wave and plane-wave Born approximations," *Phys. Rev. A*, vol. 77, p. 042701, Apr. 2008.

[8] D. Bote, F. Salvat, A. Jablonski, and C. J. Powell, "Cross sections for ionization of K, L and M shells of atoms by impact of electrons and positrons with energies up to 1 GeV: Analytical formulas," *Atom. Data Nucl. Data Tables*, vol. 95, no. 6, pp. 871–909, 2009.

[9] D. Bote, F. Salvat, A. Jablonski, and C. J. Powell, "Erratum to 'Cross sections for ionization of K, L and M shells of atoms by impact of electrons and positrons with energies up to 1 GeV. Analytical formulas' [At. Data Nucl. Data Tables 95 (2009) 871–909]," *Atom. Data Nucl. Data Tables*, vol. 97, no. 2, p. 186, 2011.

[10] Y.-K. Kim and M. E. Rudd, "Binary-encounter-dipole model for electron-impact ionization," *Phys. Rev. A*, vol. 50, pp. 3954–3967, Nov. 1994.

[11] H. Deutsch and T. D. Märk, "Calculation of absolute electron impact ionization cross-section functions for single ionization of He, Ne, Ar, Kr, Xe, N and F," *Int. J. Mass Spectrometry Ion Process.*, vol. 79, no. 3, pp. R1–R8, 1987.

[12] M. Gryziński, "Two-particle collisions. I. General relations for collisions in the laboratory system," *Phys. Rev. A*, vol. 138, pp. 305–321, Apr. 1965.

[13] E. Casnati, A. Tartari, and C. Baraldi, "An empirical approach to K-shell ionisation cross section by electrons," *J. Phys. B, At. Mol. Phys.*, vol. 15, no. 1, pp. 155–167, 1982.

[14] H. Kolbenstvedt, "Simple theory for K-ionization by relativistic electrons," *J. Appl. Phys.*, vol. 38, no. 12, pp. 4785–4787, 1967.

[15] S. M. Seltzer, "Cross sections for bremsstrahlung production and electron-impact ionization," in *Monte Carlo Transport of Electrons and Photons*, T. M. Jenkins and W. R. Nelson, Eds. New York, NY, USA: Plenum Press, 1988.

[16] C. F. von Weizsäcker, "Ausstrahlung bei Stössen sehr schneller Elektronen," *Z. Phys.*, vol. 88, nos. 9–10, pp. 612–625, 1934.

[17] C. Møller, "Zur theorie des durchgangs schneller elektronen durch materie," *Ann. Phys.*, vol. 406, no. 5, pp. 531–585, 1932.

[18] E. J. Williams, "Correlation of certain collision problems with radiation theory," *Kong. Dan. Vid. Sel. Mat. Fys. Med.*, vol. 13N4, no. 4, pp. 1–50, 1935.

[19] S. T. Perkins *et al.*, "Tables and graphs of atomic subshell and relaxation data derived from the LLNL evaluated atomic data library (EADL), $Z = 1 - 100$," Lawrence Livermore Nat. Lab., Livermore, CA, USA, Tech. Rep. UCRL-50400, 1991, vol. 30.

[20] D. E. Cullen *et al.*, "Tables and graphs of photon-interaction cross sections from 10 eV to 100 GeV derived from the LLNL Evaluated Photon Data Library (EPDL)," Lawrence Livermore Nat. Lab. UCRL-50400, vol. 6, Rev. 4, Part A: Z=1 to 50, Part B: Z=51 to 100, Livermore, CA, USA, 1989.

[21] D. E. Cullen, S. T. Perkins, and J. A. Rathkopf, "The 1989 Livermore evaluated photon data library (EPDL)," Lawrence Livermore Nat. Lab., Livermore, CA, USA, Tech. Rep. UCRL-ID-103424, 1990.

[22] D. E. Cullen, *EPICS2014: Electron Photon Interaction Cross Sections (Version 2014)*, document IAEA-NDS-218, Rev. 1, Vienna, Austria, 2015.

[23] D. E. Cullen, *A Survey of Electron Cross Section Data for use in EPICS2017*, document IAEA-NDS-226, Vienna, Austria, 2017.

[24] D. E. Cullen, *A Survey of Atomic Binding Energies for use in EPICS2017*, document IAEA-NDS-226, Vienna, Austria, 2017.

[25] M. B. Chadwick *et al.*, "ENDF/B-VII.1 nuclear data for science and technology: Cross sections, covariances, fission product yields and decay data," *Nucl. Data Sheets*, vol. 112, no. 12, pp. 2887–2996, 2011.

[26] K. Shibata *et al.*, "JENDL-4.0: A new library for nuclear science and engineering," *J. Nucl. Sci. Technol.*, vol. 48, no. 1, pp. 1–30, 2011.

[27] D. A. Brown *et al.*, "ENDF/B-VIII.0: The 8$^{\text{th}}$ major release of the nuclear reaction data library with CIELO-project cross sections, new standards and thermal scattering data," *Nucl. Data Sheets*, vol. 148, pp. 1–142, Feb. 2018.

[28] S. Agostinelli *et al.*, "Geant4—A simulation toolkit," *Nucl. Instrum. Methods Phys. Res. A, Accel. Spectrom. Detect. Assoc. Equip.*, vol. 506, no. 3, pp. 250–303, 2003.

[29] J. Allison *et al.*, "Geant4 developments and applications," *IEEE Trans. Nucl. Sci.*, vol. 53, no. 1, pp. 270–278, Feb. 2006.

[30] J. Allison *et al.*, "Recent developments in Geant4," *Nucl. Instrum. Methods Phys. Res. Section A, Accel., Spectrometers, Detect. Assoc. Equip.*, vol. 835, pp. 186–225, Nov. 2016.

[31] C. Powell *et al. NIST Standard Reference Database 164*. [Online]. Available: https://www.nist.gov/srd/nist-standard-reference-database-164

[32] F. Salvat, "PENELOPE-2014: A code system for Monte Carlo simulation of electron and photon transport," Nucl. Energy Agency, Paris, France, Tech. Rep. NEA/NSC/DOC(2015)3, 2015.

[33] Y.-K. Kim, J. P. Santos, and F. Parente, "Extension of the binary-encounter-dipole model to relativistic incident electrons," *Phys. Rev. A*, vol. 62, p. 052710, Oct. 2000.

[34] J. P. Santos, F. Parente, and Y.-K. Kim, "Cross sections for K-shell ionization of atoms by electron impact," *J. Phys. B, At. Mol. Opt. Phys.*, vol. 36, no. 21, pp. 4211–4224, 2003.

[35] H. Deutsch, P. Scheier, K. Becker, and T. D. Märk, "Revised high energy behavior of the Deutsch-Märk (DM) formula for the calculation of electron impact ionization cross sections of atoms," *Int. J. Mass Spectrometry*, vol. 233, nos. 1–3, pp. 13–17, 2004.

[36] H. Deutsch, P. Scheier, S. Matt-Leubner, K. Becker, and T. D. Märk, "A detailed comparison of calculated and measured electron-impact ionization cross sections of atoms using the Deutsch-Märk (DM) formalism," *Int. J. Mass Spectrometry*, vol. 243, no. 3, pp. 215–221, 2005.

[37] H. Deutsch, P. Scheier, S. Matt-Leubner, K. Becker, and T. D. Märk, "A detailed comparison of calculated and measured electron-impact ionization cross sections of atoms using the Deutsch–Märk (DM) formalism," *Int. J. Mass Spectrometry*, vol. 246, no. 3, pp. 215–221, 2005.

[38] H. Deutsch, K. Becker, S. Matt, and T. D. Märk, "Theoretical determination of absolute electron-impact ionization cross sections of molecules," *Int. J. Mass Spectrometry*, vol. 197, nos. 1–3, pp. 37–69, Feb. 2000.

[39] A. K. F. Haque *et al.*, "Modified version of revised Deutsch–Märk model for electron impact K-shell ionization cross-sections of atoms at relativistic energies," *Int. J. Quantum Chem.*, vol. 109, no. 7, pp. 1442–1450, 2009.

[40] W. L. Fite and R. T. Brackmann, "Collisions of electrons with hydrogen atoms. I. Ionization," *Phys. Rev.*, vol. 112, no. 1, pp. 1141–1151, 1958.

[41] J. W. McGowan, "Ionization of H(1s) near Threshold," *Phys. Rev.*, vol. 167, no. 4, pp. 43–51, 1968.

[42] E. W. Rothe, L. L. Marino, R. H. Neynaber, and S. M. Trujillo, "Electron impact ionization of atomic hydrogen and atomic oxygen," *Phys. Rev.*, vol. 125, no. 2, pp. 582–583, 1962.

[43] M. B. Shah, D. S. Elliott, and H. B. Gilbody, "Pulsed crossed-beam study of the ionisation of atomic hydrogen by electron impact," *J. Phys. B, At. Mol. Opt. Phys.*, vol. 20, no. 14, pp. 3501–3514, 1987.

[44] T. W. Shyn, "Doubly differential cross sections of secondary electrons ejected from atomic hydrogen by electron impact," *Phys. Rev. A*, vol. 45, no. 5, pp. 2951–2956, 1992.

[45] E. Krishnakumar and S. K. Srivastava, "Ionisation cross sections of rare-gas atoms by electron impact," *J. Phys. B, At. Mol. Opt. Phys.*, vol. 21, no. 6, pp. 1055–1082, 1988.

[46] R. G. Montague, M. F. A. Harrison, and A. C. H. Smith, "A measurement of the cross section for ionisation of helium by electron impact using a fast crossed beam technique," *J. Phys. B, At. Mol. Opt. Phys.*, vol. 17, no. 16, pp. 3295–3310, 1984.

[47] P. Nagy, A. Skutlartz, and V. Schmidt, "Absolute ionisation cross sections for electron impact in rare gases," *J. Phys. B, At. Mol. Opt. Phys.*, vol. 13, no. 6, pp. 1249–1267, 1980.

[48] D. Rapp and P. Englander-Golden, "Total cross sections for ionization and attachment in gases by electron impact. I. Positive ionization," *J. Chem. Phys.*, vol. 43, no. 5, pp. 1464–1479, 1965.

[49] B. L. Schram, F. J. De Heer, M. J. van der Wiel, and J. Kistemaker, "Ionization cross sections for electrons (0.6–20 keV) in noble and diatomic gases," *Physica*, vol. 31, no. 1, pp. 94–112, 1965.

[50] B. L. Schram, A. J. H. Boerboom, and J. Kistemaker, "Partial ionization cross sections of noble gases for electrons with energy 0.5–16 keV.: I. Helium and neon," *Physica*, vol. 32, no. 2, pp. 185–196, 1966.

[51] B. L. Schram, H. R. Moustafa, J. Schutten, and F. J. de Heer, "Ionization cross sections for electrons (100–600 eV) in noble and diatomic gases," *Physica*, vol. 32, no. 4, pp. 734–740, 1966.

[52] M. B. Shah, D. S. Elliott, P. McCallion, and H. B. Gilbody, "Single and double ionisation of helium by electron impact," *J. Phys. B, At. Mol. Opt. Phys.*, vol. 21, no. 15, pp. 2751–2761, 1988.

[53] K. Stephan, H. Helm, and T. D. Märk, "Mass spectrometric determination of partial electron impact ionization cross sections of He, Ne, Ar and Kr from threshold up to 180 eV," *J. Chem. Phys.*, vol. 73, no. 8, pp. 3763–3778, 1980.

[54] R. C. Wetzel, F. A. Baiocchi, T. R. Hayes, and R. S. Freund, "Absolute cross sections for electron-impact ionization of the rare-gas atoms by the fast-neutral-beam method," *Phys. Rev. A*, vol. 35, no. 2, pp. 559–577, 1987.

[55] R. F. Egerton, "Inelastic scattering of 80 keV electrons in amorphous carbon," *Philos. Mag.*, vol. 31, no. 1, pp. 199–215, 1975.

[56] R. L. Gerlach and A. R. DuCharme, "Total electron impact ionization cross sections of K shells of surface atoms," *Surf. Sci.*, vol. 32, pp. 329–340, 1972.

[57] W. Hink and H. Paschke, "K-shell-fluorescence yield for carbon and other light elements," *Phys. Rev. A*, vol. 4, no. 2, pp. 507–511, 1971.

[58] M. Isaacson, "Interaction of 25 keV electrons with the nucleic acid bases, adenine, thymine, and uracil. II. Inner shell excitation and inelastic scattering cross sections," *J. Chem. Phys.*, vol. 56, no. 5, pp. 1813–1818, 1972.

[59] S. P. Limandri, M. A. Z. Vasconcellos, R. Hinrichs, and J. C. Trincavelli, "Experimental determination of cross sections for K-shell ionization by electron impact for C, O, Al, Si, and Ti," *Phys. Rev. A*, vol. 86, no. 4, p. 042701, 2012.

[60] H. Tawara, K. G. Harrison, and F. J. De Heer, "X-ray emission cross sections and fluorescence yields for light atoms and molecules by electron impact," *Physica*, vol. 63, no. 2, pp. 351–367, 1973.

[61] G. Glupe and W. Mehlhorn, "Absolute electron impact ionization cross sections of N, O and Ne," *J. Phys.*, vol. 32, no. C4, pp. 40–43, 1971.

[62] H. Platten, G. Schiwietz, and G. Nolte, "Cross sections for K-shell ionization of Si and Ar by 4 keV to 10 keV electron impact," *Phys. Lett. A*, vol. 107, no. 2, pp. 83–86, 1985.

[63] H. Tawara *et al.*, "K-shell ionization by relativistic electron impact," *Phys. Lett. A*, vol. 54, no. 2, pp. 171–173, 1975.

[64] M. Kamiya, A. Kuwako, K. Ishii, S. Morita, and M. Oyamada, "Density effect in K-shell ionization by ultrarelativistic electrons," *Phys. Rev. A*, vol. 22, no. 2, pp. 413–420, 1980.

[65] D. H. H. Hoffmann, C. Brendel, H. Genz, W. Löw, S. Müller, and A. Richter, "Inner-shell ionization by relativistic electron impact," *Zeitschrift Phys. A, Atoms Nucl.*, vol. 293, no. 3, pp. 187–201, 1979.

[66] S. C. McDonald and B. M. Spicer, "Density effect in K-shell ionization by relativistic electron impact," *Phys. Rev. A*, vol. 37, no. 3, pp. 985–987, 1988.

[67] K. Fennane *et al.*, "Double K-shell ionization of Al induced by photon and electron impact," *Phys. Rev. A*, vol. 79, no. 3, p. 032708, 2009.

[68] W. Hink and A. Ziegler, "Der Wirkungsquerschnitt für die Ionisierung der K-Schale von Aluminium durch ElektronenstoSS (3–30 keV)," *Zeitschrift Phys. Hadrons Nucl.*, vol. 226, no. 3, pp. 222–234, 1969.

[69] K. Ishii *et al.*, "Inner-shell ionization by ultrarelativistic electrons," *Phys. Rev. A*, vol. 15, no. 3, pp. 906–913, 1977.

[70] O. Mauron and J.-C. Dousse, "Double KL ionization in Al, Ca, and Co targets bombarded by low-energy electrons," *Phys. Rev. A*, vol. 66, no. 4, p. 042713, 2002.

[71] C. S. Mei *et al.*, "Measurements of K-shell ionization cross sections of Al and L-shell X-ray production cross sections of Se by intermediate-energy electron impact," *J. Phys. B, At. Mol. Opt. Phys.*, vol. 49, no. 24, p. 245204, 2016.

[72] G. L. Westbrook and C. A. Quarles, "Total cross sections for ionization of the K-shell by electron bombardment," *Nucl. Instrum. Methods Phys. Res. B, Beam Interact. Mater. At.*, vols. 24–25, pp. 196–198, Apr. 1987.

[73] A. V. Shchagin, V. I. Pristupa, and N. A. Khizhnyak, "K-shell ionization cross section of Si atoms by relativistic electrons," *Nucl. Instrum. Methods Phys. Res. B, Beam Interact. Mater. At.*, vol. 84, no. 1, pp. 9–13, 1994.

[74] J. Zhu, Z. An, M. Liu, and L. Tian, "Measurements of the K-shell ionization cross sections of Si by 3–25 keV electron impact using the thick-target method," *Phys. Rev. A*, vol. 79, no. 5, p. 052710, 2009.

[75] Y. Wu, Z. An, Y. M. Duan, and M. T. Liu, "Measurements of K-shell ionization cross-sections of S, Ca and Zn by 7–30 keV electron impact," *Nucl. Instrum. Methods Phys. Res. B, Beam Interact. Mater. At.*, vol. 268, no. 17, pp. 2820–2824, 2010.

[76] Y. Wu, Z. An, Y. M. Duan, M. T. Liu, and J. Wu, "K-shell ionization cross sections of Cl and L_α, L_β X-ray production cross sections of Ba by 6–30 keV electron impact," *Nucl. Instrum. Methods Phys. Res. B, Beam Interact. Mater. At.*, vol. 269, no. 2, pp. 117–121, 2011.

[77] R. Hippler, K. Saeed, I. McGregor, and H. Kleinpoppen, "Energy dependence of characteristic and bremsstrahlung cross sections of argon induced by electron bombardment at low energies," *Zeitschrift Phys. A, Atoms Nucl.*, vol. 307, no. 1, pp. 83–87, 1982.

[78] R. Hippler, H. Klar, K. Saeed, I. McGregor, A. J. Duncan and H. Kleinpoppen, "Threshold behaviour of Ar K and Xe L3 ionisation by electron impact," *J. Phys. B, At. Mol. Opt. Phys.*, vol. 16, no. 20, pp. L617–L621, 1983.

[79] D. H. H. Hoffmann, H. Genz, W. Löw, and A. Richter, "Z and E dependence and scaling behaviour of the K-shell ionization cross section for relativistic electron impact," *Phys. Lett. A*, vol. 65, no. 4, pp. 304–306, 1978.

[80] C. Quarles and M. Semaan, "Characteristic X-ray production by electron bombardment of argon, krypton, and xenon from 4 to 10 keV," *Phys. Rev. A*, vol. 26, no. 6, pp. 3147–3151, 1982.

[81] R. K. Singh and R. Shanker, "The emission of characteristic and non-characteristic X-rays from collisions of 10–22 keV electrons with argon," *J. Phys. B, At. Mol. Opt. Phys.*, vol. 36, pp. 3031–3042, 2003.

[82] V. P. Shevelko, A. M. Solomon, and V. S. Vukstich, "K-shell ionization of free metal atoms K, Ca, Rb and Sr by electron impact," *Phys. Scripta*, vol. 43, no. 2, pp. 158–161, 1991.

[83] Y. Wu, Z. An, Y. M. Duan, M. T. Liu, and X. P. Ouyang, "K-shell ionization cross sections of K and Lα X-ray production cross sections of I by 10–30 keV electron impact," *Can. J. Phys.*, vol. 90, no. 2, pp. 125–130, 2012.

[84] Z. An, C. H. Tang, C. G. Zhou, and Z. M. Luo, "Measurement of scandium and vanadium K-shell ionization cross sections by electron impact," *J. Phys. B, At. Mol. Opt. Phys.*, vol. 33, no. 18, pp. 3677–3684, 2000.

[85] Z. An, Z. M. Luo, and C. Tang, "Study of cross-sections for the K-shell ionization of atoms by electron and positron impact," *Nucl. Instrum. Methods Phys. Res. B, Beam Interact. Mater. At.*, vol. 179, no. 3, pp. 334–342, 2001.

[86] T. H. Li, Z. An, and Z. M. Luo, "Measurement of Sc and V K-shell ionization cross sections by slow electron impact," *Nucl. Sci. Tech.*, vol. 7, no. 4, pp. 228–231, 1996.

[87] Z. An *et al.*, "Some recent progress on the measurement of K-shell ionization cross-sections of atoms by electron impact: Application to Ti and Cr elements," *Nucl. Instrum. Methods Phys. Res. B, Beam Interact. Mater. At.*, vol. 207, no. 3, pp. 268–274, 2003.

[88] F. Q. He, X. F. Peng, X. G. Long, Z. M. Luo, and Z. An, "K-shell ionization cross sections by electron bombardment at low energies," *Nucl. Instrum. Methods Phys. Res. B, Beam Interact. Mater. At.*, vol. 129, no. 4, pp. 445–450, 1997.

[89] J. Jessenberger and W. Hink, "Absolute electron impact$K$-ionization cross sections of titanium and nickel ($\leqq$50 keV)," *Z. Phys. A*, vol. 275, no. 4, pp. 331–337, 1975.

[90] C. Tang, Z. Luo, Z. An, F. He, X. Peng, and X. Long, "The atomic K- and L-shell ionization cross-sections by electron impact," in *Advanced Diagnostics for Magnetic and Inertial Fusion*. New York, NY, USA: Springer, 2002, pp. 233–236.

[91] Y. Watanabe, T. Kubozoe, T. Tomimasu, T. Mikado, and T. Yamazaki, "K-shell ionization by relativistic electron impact," *Phys. Rev. A*, vol. 35, no. 3, pp. 1423–1425, 1987.

[92] W. Scholz and A. Li-Scholz, "K-shell ionization cross sections for 2.04-MeV electrons," *Phys. Rev. Lett.*, vol. 29, no. 12, pp. 761–764, 1972.

[93] Z. An, C. H. Tang, and Z. M. Luo, "Measurement of K-shell ionization cross sections of Cr, Ni and Cu atoms by 7.5–25 keV electron impact," *Chin. Phys. Lett.*, vol. 18, no. 11, pp. 1460–1462, 2001.

[94] X. Llovet, C. Merlet, and F. Salvat, "Measurements of K-shell ionization cross sections of Cr, Ni, and Cu by impact of 6.5–40 keV electrons," *J. Phys. B, At. Mol. Opt. Phys.*, vol. 33, no. 18, pp. 3761–3772, 2000.

[95] Z. Luo, Z. An, F. He, T. Li, X. Long, and X. Peng, "Correction of the influence of the substrate upon the measurement of K-shell ionization cross sections," *J. Phys. B, At. Mol. Opt. Phys.*, vol. 29, no. 17, pp. 4001–4005, 1996.

[96] J. Colgan, C. J. Fontes, and H. L. Zhang, "Inner-shell electron-impact ionization of neutral atoms," *Phys. Rev. A*, vol. 73, p. 062711, 2001.

[97] B. Fischer and K.-W. Hoffmann, "Die intensität der bremsstrahlung und der charakteristischenK-Röntgenstrahlung dünner anoden," *Zeitschrift Physik*, vol. 204, no. 2, pp. 122–128, 1967.

[98] X. Llovet, C. Merlet, and F. Salvat, "Measurement of absolute cross sections for K-shell ionization of Fe and Mn by electron impact," *J. Phys. B, At. Mol. Opt. Phys.*, vol. 35, no. 4, pp. 973–982, 2002.

[99] Z. Luo, Z. An, T. Li, L. Wang, Q. Zhu, and X. Xia, "Measurement of K-shell ionization cross sections of Fe and Mn by electron impact," *J. Phys. B, At. Mol. Opt. Phys.*, vol. 30, no. 11, pp. 2681–2686, 1997.

[100] K. Shima, "Mn and Cu K-shell ionization cross sections by slow electron impact," *Phys. Lett. A*, vol. 77, no. 4, pp. 237–239, 1980.

[101] C. Tang, Z. An, T. Li, and Z. Luo, "Measurement of zinc and manganese K-shell ionization cross-sections by electron impact," *Nucl. Instrum. Methods Phys. Res. B, Beam Interact. Mater. At.*, vol. 155, nos. 1–2, pp. 1–5, 1999.

[102] F.-Q. He, X.-G. Long, X.-F. Peng, Z.-M. Luo, and Z. An, "K-shell ionization of iron by electron bombardment," *Acta Phys. Sinica*, vol. 5, no. 7, pp. 499–504, 1996.

[103] F.-Q. He, X.-G. Long, X.-F. Peng, Z.-M. Luo, and Z. An, "K-shell ionization of molybdenum and iron by electron bombardment," *Chin. Phys. Lett.*, vol. 13, no. 3, pp. 175–177, 1996.

[104] Z. An, T. H. Li, L. M. Wang, X. Y. Xia, and Z. M. Luo, "Correction of substrate effect in the measurement of 8–25-keV electron-impact K-shell ionization cross sections of Cu and Co elements," *Phys. Rev. A*, vol. 54, no. 4, pp. 3067–3069, 1996.

[105] Z. An, Y. Wu, M. T. Liu, Y. M. Duan, and C. H. Tang, "Thick-target method in the measurement of inner-shell ionization cross-sections by low-energy electron impact," *Nucl. Instrum. Methods Phys. Res. B, Beam Interact. Mater. At.*, vol. 246, no. 2, pp. 281–287, 2006.

[106] G. R. Dangerfield and B. M. Spicer, "K-shell ionization by relativistic electrons," *J. Phys. B, At. Mol. Opt. Phys.*, vol. 8, no. 10, pp. 1744–1751, 1975.

[107] H. Genz *et al.*, "Search for the density effect in inner-shell lonization by ultra relativistic electron impact," *Z. Phys. A, Atoms Nucl.*, vol. 305, no. 1, pp. 9–19, 1982.

[108] J. W. Motz and R. C. Placious, "K-ionization cross sections for relativistic electrons," *Phys. Rev.*, vol. 136, no. 3A, pp. A662–A665, 1964.

[109] L. T. Pockman, D. L. Webster, P. Kirkpatrick, and K. Harworth, "The probability of K ionization of nickel by electrons as a function of their energy," *Phys. Rev.*, vol. 71, no. 6, pp. 330–338, 1947.

[110] S. A. H. Seif el Nasr, D. Berényi, and G. Bibok, "Inner shell ionization cross sections for relativistic electrons," *Z. Phys.*, vol. 267, no. 3, pp. 169–174, 1974.

[111] A. E. Smick and P. Kirkpatrick, "Absolute K-ionization cross section of the nickel atom under electron bombardment at 70 kv," *Phys. Rev.*, vol. 67, nos. 5–6, pp. 153–161, 1945.

[112] R. Gauvin and G. L'Esperance, "The measurement of inner-shell ionization cross sections by electron impact in a TEM," in *Proc. 50th Annu. Meeting EMSA*, 1945, p. 1266.

[113] D. Berenyi, G. Hock, S. Ricz, B. Schlenk, and A. Valek, "Kα/Kβ X-ray intensity ratios and K-shell ionization cross sections for bombardment by electrons of 300-600 keV," *J. Phys. B, At. Mol. Opt. Phys.*, vol. 11, no. 4, pp. 709–713, 1978.

[114] D. V. Davis, V. D. Mistry, and C. A. Quarles, "Inner shell ionization of copper, silver and gold by electron bombardment," *Phys. Lett. A*, vol. 38, no. 3, pp. 169–170, 1972.

[115] H. Hubner, K. Ilgen, and K. W. Hoffmann, "Effective cross-section of ionization in the K-shell by electron impact," *Z. Phys.*, vol. 255, no. 3, pp. 269–280, 1972.

[116] L. M. Middleman, R. L. Ford, and R. Hofstadter, "Measurement of cross sections for X-ray production by high-energy electrons," *Phys. Rev. A*, vol. 2, no. 4, pp. 1429–1443, 1970.

[117] K. Shima, T. Nakagawa, K. Umetani, and T. Mikumo, "Threshold behavior of Cu-, Ge-, Ar-K-, and Au-L_3-shell ionization cross sections by electron impact," *Phys. Rev. A*, vol. 24, no. 1, pp. 72–78, 1981.

[118] C.-G. Zhou, Z. An, and Z.-M. Luo, "Measurement and correction of K-shell ionization cross sections for copper and gallium by electron impact," *Chin. Phys. Lett.*, vol. 18, no. 6, pp. 759–760, 2001.

[119] C. Merlet, X. Llovet, and J. M. Fernandez-Varea, "Absolute K-shell ionization cross sections and Lα and Lβ_1 X-ray production cross sections of Ga and As by 1.5–39-keV electrons," *Phys. Rev. A*, vol. 73, no. 6, p. 062719, 2006.

[120] C. Zhou, Z. An, and Z. Luo, "Measurement of K-shell production cross sections for Ga, Ge and Zr elements by electron impact," *J. Phys. B, At. Mol. Opt. Phys.*, vol. 35, no. 4, pp. 841–845, 2002.

[121] C. Merlet, X. Llovet, and F. Salvat, "Measurements of absolute K-shell ionization cross sections and L-shell X-ray production cross sections of Ge by electron impact," *Phys. Rev. A*, vol. 69, no. 3, p. 032708, 2004.

[122] C. Tang, Z. An, Z. Luo, and M. Liu, "Measurements of germanium K-shell ionization cross sections and tin L-shell X-ray production cross sections by electron impact," *J. Appl. Phys.*, vol. 91, no. 10, pp. 6739–6743, 2002.

[123] K. Kiss, G. Kalman, J. Palinkas, and B. Schlenk, "Investigation of inner-shell ionization by electron impact in the 60–600 keV energy region," *Acta Phys. Acad. Sci. Hungaricae*, vol. 50, no. 1, pp. 97–102, 1981.

[124] Z. Luo, T. Changhuan, A. Zhu, H. Fuqing, P. Xiufeng, and L. Xianguan, "Selenium and yttrium K-shell ionization cross-sections by electron impact," *Phys. Rev. A*, vol. 63, no. 3, p. 034702, 2001.

[125] H. Hansen, H. Weigmann, and A. Flammersfeld, "Messung des wirkungsquerschnitts für K-ionisierung durch negatonen-und positonenstoß," *Nucl. Phys.*, vol. 58, pp. 241–253, Sep. 1964.

[126] X. Peng, F. He, X. Long, Z. Luo, and Z. An, "Cross sections for *K*-shell ionization of niobium by electron impact," *Phys. Rev. A*, vol. 58, no. 3, pp. 2034–2036, 1998.

[127] F. Q. He, X. G. Long, X. F. Peng, Z. M. Luo, and Z. An, "K-shell ionization of molybdenum by electron bombardment," *Nucl. Instrum. Methods Phys. Res. B, Beam Interact. Mater. At.*, vol. 114, nos. 3–4, pp. 213–216, 1996.

[128] K. H. Berkner, S. N. Kaplan, and R. V. Pyle, "Cross sections for *K*-shell ionization of Pd and Au by 2.5 and 7.1 MeV electrons," *Bull. Amer. Phys. Soc.*, vol. 15, p. 786, 1970.

[129] S. Ricz, B. Schlenk, D. Berenyi, G. Hock, and A. Valek, "*K*-shell ionization cross sections of Pd, Ag, In and Sn for relativistic electrons," *Acta Phys. Acad. Sci. Hungaricae*, vol. 42, no. 3, pp. 269–271, 1977.

[130] J. C. Clark, "A measurement of the absolute probability of *K*-electron ionization of silver by cathode rays," *Phys. Rev.*, vol. 48, no. 1, pp. 30–42, 1935.

[131] H. Hansen and A. Flammersfeld, "Messung des wirkungsquerschnitts für K-ionisierung durch stoss niederenergetischer negatonen und positonen," *Nucl. Phys.*, vol. 79, no. 1, pp. 135–144, 1966.

[132] R. Hippler *et al.*, "Multiple and inner-shell ionization by positron and electron impact," *Nucl. Instrum. Methods Phys. Res. B, Beam Interact. Mater. At.*, vol. 99, nos. 1–4, pp. 12–14, 1995.

[133] D. H. Rester and W. E. Dance, "*K*-shell ionization of Ag, Sn, and Au from electron bombardment," *Phys. Rev.*, vol. 152, no. 1, pp. 1–3, 1966.

[134] B. Schlenk, D. Berényi, S. Ricz, A. Valek, and G. Hock, "Inner-shell ionization by electrons in the 300–600 keV region," *Acta Phys. Acad. Sci. Hungaricae*, vol. 41, no. 3, pp. 159–163, 1976.

[135] H. Schneider, I. Tobehn, F. Ebel, and R. Hippler, "Absolute cross sections for inner shell ionization by lepton impact," *Phys. Rev. Lett.*, vol. 71, no. 17, pp. 2707–2709, 1993.

[136] H. Schneider, I. Tobehn, R. Hippler, and F. Ebel, "Absolute cross-section measurements of inner-shell ionization," *Hyperfine Interact.*, vol. 89, no. 1, pp. 119–125, 1994.

[137] V. R. Vanin, M. V. M. Guevara, N. L. Maidana, M. N. Martins, and J. M. Fernández-Varea, "Ag K-shell ionization by electron impact: New cross-section measurements between 50 and 100 keV and review of previous experimental data," *Radiat. Phys. Chem.*, vol. 119, pp. 14–23, Feb. 2016.

[138] Z. Chang-Geng, F. Yu-Chuan, A. Zhu, T. Chang-Huan, and L. Zheng-Ming, "Measurement and multiple scattering correction of K-shell ionization cross sections of silver by electron impact," *Chin. Phys. Lett.*, vol. 18, no. 4, pp. 531–532, 2001.

[139] J. M. Fernández-Varea, V. Jahnke, N. L. Maidana, A. A. Malafronte, and V. R. Vanin, "Cross sections of K-shell ionization by electron impact, measured from threshold to 100 keV, for Au and Bi," *J. Phys. B, At. Mol. Opt. Phys.*, vol. 47, no. 15, p. 155201, 2014.

[140] S. Reusch, H. Genz, W. Löw, and A. Richter, "A method to determine L-subshell ionization cross sections for medium and heavy elements," *Zeitschrift Phys. D Atoms, Mol. Clusters*, vol. 3, no. 4, pp. 379–389, 1986.

[141] A. Sepúlveda, A. P. Bertol, M. A. Z. Vasconcellos, J. Trincavelli, R. Hinrichs, and G. Castellano, "Silver L_1, L_2 and L_3 cross-sections for ionization and X-ray production by electron impact," *J. Phys. B, At. Mol. Opt. Phys.*, vol. 47, no. 21, p. 215006, 2014.

[142] R. Hippler, I. McGregor, M. Aydinol, and H. Kleinpoppen, "Ionization of xenon *L* subshells by low-energy electron impact," *Phys. Rev. A*, vol. 23, no. 4, pp. 1730–1736, 1981.

[143] Y. K. Park, M. T. Smith, and W. Scholz, "Cross sections for *L* X-ray production and *L*-subshell ionization by MeV electrons," *Phys. Rev. A*, vol. 12, no. 4, pp. 1358–1364, 1975.

[144] C.-N. Chang, "*L*-subshell ionization cross sections for tungsten at low electron energies," *Phys. Rev. A*, vol. 19, no. 5, pp. 1930–1935, 1979.

[145] S. F. Barros, V. R. Vanin, N. L. Maidana, and J. M. Fernández-Varea, "Ionization cross sections of the *L* subshells of Au by 50 to 100 keV electron impact," *J. Phys. B, At., Mol. Opt. Phys.*, vol. 48, no. 17, p. 175201, 2015.

[146] J. Pálinkás and B. Schlenk, "*L*-subshell ionization cross sections for Au, Pb, and Bi by 60–600 keV electron impact," *Zeitschrift Phys. Atoms Nuclei*, vol. 297, no. 1, pp. 29–33, 1980.

[147] H. V. Rahangdale *et al.*, "Determination of subshell-resolved *L* shell-ionization cross sections of gold induced by 15–40 keV electrons," *Phys. Rev. A*, vol. 89, p. 052708, May 2014.

[148] H. V. Rahangdale *et al.*, "Spectroscopic investigations of *L*-shell ionization in heavy elements by electron impact," *J. Quant. Spectrosc. Radiat. Transf.*, vol. 174, pp. 79–87, May 2014.

[149] M. Green, "The angular distribution of characteristic X radiation and its origin within a solid target," *Proc. Phys. Soc.*, vol. 83, no. 3, pp. 435–451, 1964.

[150] M. Green and V. E. Cosslett, "Measurements of K, L and M shell X-ray production efficiencies," *J. Phys. D, Appl. Phys.*, vol. 1, no. 4, pp. 425–436, 1968.

[151] B. B. Kinsey, "The emission of L radiation following internal conversion of γ-radiation in heavy elements," *Canad. J. Res.*, vol. 26, no. 6, pp. 404–420, 1948.

[152] H. Küstner and E. Arends, "Ausbeutekoeffizienten, Intensitätsverhältnisse und Absorptionswahrscheinlichkeiten in der L-Serie der Schwerelemente," *Ann. Phys.*, vol. 414, no. 5, pp. 443–472, 1935.

[153] L. Pincherle, "L'effetto auger," *II Nuovo Cimento*, vol. 12, no. 2, pp. 81–92, 1935.

[154] S. I. Salem and L. D. Moreland, "L_{II} and L_{III} ionization cross sections in gold at very low energies," *Phys. Lett. A*, vol. 37, no. 2, pp. 161–162, 1971.

[155] G. P. Li, T. Takayanagi, K. Wakiya, and H. Suzuki, "Cross section for 3*s* ionization in argon by electron impact," *Phys. Rev. A*, vol. 38, no. 4, pp. 1831–1838, 1988.

[156] A. Moy, C. Merlet, X. Llovet, and O. Dugne, "M-subshell ionization cross sections of U by electron impact," *J. Phys. B, At., Mol. Opt. Phys.*, vol. 47, no. 5, p. 055202, 2014.

[157] A. Yagishita, "Ionization cross sections of Krypton M subshells by electron impact," *Phys. Lett. A*, vol. 87, no. 1, pp. 30–32, 1981.

[158] M. Liu, Z. An, C. Tang, Z. Luo, X. Peng, and X. Long, "Experimental electron-impact *K*-shell ionization cross sections," *At. Data Nucl. Data Tables*, vol. 76, no. 2, pp. 213–234, 2000.

[159] A. Wald and J. Wolfowitz, "An exact test for randomness in the non-parametric case based on serial correlation," *Ann. Math. Stat.*, vol. 14, no. 4, pp. 378–388, 1943.

[160] R. K. Bock and W. Krischer, *The Data Analysis BriefBook*. Berlin, Germmany: Springer, 1998.

[161] M. Mitchell. *Engauge Digitizer*. [Online]. Available: https://-github.com/markummitchell/engauge-digitizer/

[162] J. A. Huwaldt. *PlotDigitizer*. [Online]. Available: https://source-forge.net/projects/plotdigitizer/

[163] W. Bambynek *et al.*, "X-ray fluorescence yields, auger, and Coster–Kronig transition probabilities," *Rev. Mod. Phys.*, vol. 44, no. 4, pp. 716–813, 1972.

[164] M. O. Krause, "Atomic radiative and radiationless yields for *K* and *L* shells," *J. Phys. Chem. Reference Data*, vol. 8, no. 2, pp. 307–327, 1979.

[165] J. H. Hubbell *et al.*, "A review, bibliography, and tabulation of K, L, and higher atomic shell X-Ray fluorescence yields," *J. Phys. Chem. Reference Data*, vol. 23, no. 2, pp. 339–364, 1994.

[166] J. H. Hubbell, "Erratum: 'A review, bibliography, and tabulation of K, L, and higher atomic shell X-Ray fluorescence yields,"' *J. Phys. Chem. Reference Data*, vol. 33, no. 2, p. 621, 2004.

[167] S. Daoudi *et al.*, "New K-shell fluorescence yields curve for elements with $3 \leq Z \leq 99$," *J. Korean Phys. Soc.*, vol. 67, no. 9, pp. 1537–1543, 2015.

[168] W. T. Elam *et al.*, "A new atomic database for X-ray spectroscopic calculations," *Radiat. Phys. Chem.*, vol. 63, no. 2, pp. 121–128, 2002.

[169] A. Kahoul *et al.*, "K-shell fluorescence yields for elements with $6 \leq Z \leq 99$," *Radiat. Phys. Chem.*, vol. 80, no. 3, pp. 369–377, 2011.

[170] A. Kahoul, V. Aylikci, N. K. Aylikci, E. Cengiz, and G. Apaydind, "Updated database and new empirical values for K-shell fluorescence yields," *Radiat. Phys. Chem.*, vol. 81, no. 7, pp. 713–727, 2012.

[171] D. Sanchez del Rio and R. J. Jesus, "XOP v2.4: Recent developments of the X-ray optics software toolkit," in *Proc. SPIE Opt. Eng. App.*, San Diego, CA, USA, 2011.

[172] J. H. Hubbell, "Bibliography and current status of K, L, and higher shell fluorescence yields for computations of photon energy-absorption coefficients," NIST, Gaithersburg, MD, USA, Tech. Rep. NISTIR 89-4144, 1989.

[173] W. Bambynek, "A new evaluation of k-shell fluorescence yields," in *Proc. Int. Conf. X-ray Inner-Shell Processes Atoms, Molecules Solids*, 1984, pp. 1–2.

[174] A. Alexandrescu, *Modern C++ Design*. Reading, MA, USA: Addison-Wesley, 2001.

[175] *IEEE Standard for System, Software, and Hardware Verification and Validation*, IEEE Standard 1012-2016, 2017.

[176] A. G. Frodesen, O. Skjeggestad, and H. Tofte, *Probability and Statistics in Particle Physics*. Bergen, Norway: Universitetsforlaget, 1979.
[177] M. Paterno, "Calculating efficiencies and their uncertainties," Batavia, IL, USA, Tech. Rep. FERMILAB-TM-2286-CD, 2004.
[178] G. Cowan. (2008). *Error Analysis for Efficiency*. [Online]. Available: http://www.pp.rhul.ac.uk/cowan/stat/notes/efferr.pdf
[179] T. W. Anderson and D. A. Darling, "Asymptotic theory of certain 'goodness of fit' criteria based on stochastic processes," *Ann. Math. Stat.*, vol. 23, no. 2, pp. 193–212, 1952.
[180] T. W. Anderson and D. A. Darling, "A test of goodness of fit," *J. Amer. Stat. Assoc.*, vol. 49, no. 268, pp. 765–769, 1954.
[181] H. Cramér, "On the composition of elementary errors. Second paper: Statistical applications," *Skand. Aktuarietidskr.*, vol. 11, pp. 13–74 and 141–180, 1928.
[182] R. von Mises, *Wahrscheinlichkeitsrechnung und Ihre Anwendung in der Statistik und Theoretischen Physik*. Leipzig, Germany: F. Duticke, 1931.
[183] A. N. Kolmogorov, "Sulla determinazione empirica di una lgge di distribuzione," *Gior. Ist. Ital. Attuari*, vol. 4, pp. 83–91, 1933.
[184] N. V. Smirnov, "On the estimation of the discrepancy between empirical curves of distribution for two independent samples," *Bull. Math. Univ. Moscow*, vol. 2, no. 2, pp. 3–14, 1939.
[185] K. Pearson, "On the χ^2 test of goodness of fit," *Biometrika*, vol. 14, nos. 1–2, pp. 186–191, 1922.
[186] R. A. Fisher, "On the interpretation of χ^2 from contingency tables, and the calculation of P," *J. Roy. Stat. Soc.*, vol. 85, no. 1, pp. 87–94, 1922.
[187] S. Suissa and J. J. Shuster, "Exact unconditional sample sizes for the 2 × 2 binomial trial," *J. Roy. Stat. Soc. A (Gen.)*, vol. 148, no. 4, pp. 317–327, 1985.
[188] G. A. Barnard, "Significance tests for 2 × 2 tables," *Biometrika*, vol. 34, nos. 1–2, pp. 123–138, 1947.
[189] R. D. Boschloo, "Raised conditional level of significance for the 2 × 2-table when testing the equality of two probabilities," *Stat. Neerlandica*, vol. 24, no. 1, pp. 1–9, 1970.
[190] R. C. Team. (2018). R: A language and environment for statistical computing. R Foundation for Statistical Computing, Vienna, Austria. [Online]. Available: http://www.R-project.org/
[191] G. A. P. Cirrone *et al.*, "A Goodness-of-Fit Statistical Toolkit," *IEEE Trans. Nucl. Sci.*, vol. 51, no. 5, pp. 2056–2063, Oct. 2004.
[192] B. Mascialino, A. Pfeiffer, M. G. Pia, A. Ribon, and P. Viarengo, "New developments of the goodness-of-fit statistical toolkit," *IEEE Trans. Nucl. Sci.*, vol. 53, no. 6, pp. 3834–3841, Dec. 2006.
[193] M. C. Han *et al.*, "Validation of cross sections for Monte Carlo simulation of the photoelectric effect," *IEEE Trans. Nucl. Sci.*, vol. 63, no. 2, pp. 1117–1146, Apr. 2016.
[194] T. Basaglia *et al.*, "Quantitative test of the evolution of geant4 electron backscattering simulation," *IEEE Trans. Nucl. Sci.*, vol. 63, no. 6, pp. 2849–2865, Dec. 2016.
[195] T. Basaglia *et al.*, "Experimental assessment of electron ionization cross sections," in *Proc. IEEE Nucl. Sci. Symp. Med. Imag. Conf. Room-Temp. Semiconductor Detector Workshop (NSS/MIC/RTSD)*. Oct./Nov. 2016, pp. 1–3, doi: 10.1109/NSSMIC.2016.8069822.
[196] A. Agresti, "A survey of exact inference for contingency tables," *Stat. Sci.*, vol. 7, no. 1, pp. 131–153, 1992.